NASA/TM–2000–209965

A Coupled Ocean General Circulation, Biogeochemical, and Radiative Model of the Global Oceans: Seasonal Distributions of Ocean Chlorophyll and Nutrients

Waston W. Gregg

September 2000

The NASA STI Program Office ... in Profile

Since its founding, NASA has been dedicated to the advancement of aeronautics and space science. The NASA Scientific and Technical Information (STI) Program Office plays a key part in helping NASA maintain this important role.

The NASA STI Program Office is operated by Langley Research Center, the lead center for NASA's scientific and technical information. The NASA STI Program Office provides access to the NASA STI Database, the largest collection of aeronautical and space science STI in the world. The Program Office is also NASA's institutional mechanism for disseminating the results of its research and development activities. These results are published by NASA in the NASA STI Report Series, which includes the following report types:

- TECHNICAL PUBLICATION. Reports of completed research or a major significant phase of research that present the results of NASA programs and include extensive data or theoretical analysis. Includes compilations of significant scientific and technical data and information deemed to be of continuing reference value. NASA's counterpart of peer-reviewed formal professional papers but has less stringent limitations on manuscript length and extent of graphic presentations.
- TECHNICAL MEMORANDUM. Scientific and technical findings that are preliminary or of specialized interest, e.g., quick release reports, working papers, and bibliographies that contain minimal annotation. Does not contain extensive analysis.
- CONTRACTOR REPORT. Scientific and technical findings by NASA-sponsored contractors and grantees.
- CONFERENCE PUBLICATION. Collected papers from scientific and technical conferences, symposia, seminars, or other meetings sponsored or cosponsored by NASA.
- SPECIAL PUBLICATION. Scientific, technical, or historical information from NASA programs, projects, and mission, often concerned with subjects having substantial public interest.
- TECHNICAL TRANSLATION. English-language translations of foreign scientific and technical material pertinent to NASA's mission.

Specialized services that complement the STI Program Office's diverse offerings include creating custom thesauri, building customized databases, organizing and publishing research results . . . even providing videos.

For more information about the NASA STI Program Office, see the following:

- Access the NASA STI Program Home Page at http://www.sti.nasa.gov/STI-homepage.html
- E-mail your question via the Internet to help@sti.nasa.gov
- Fax your question to the NASA Access Help Desk at (301) 621-0134
- Telephone the NASA Access Help Desk at (301) 621-0390
- Write to:
  NASA Access Help Desk
  NASA Center for AeroSpace Information
  7121 Standard Drive
  Hanover, MD 21076–1320

NASA/TM–2000–209965

A Coupled Ocean General Circulation, Biogeochemical, and Radiative Model of the Global Oceans: Seasonal Distributions of Ocean Chlorophyll and Nutrients

Waston W. Gregg
Laboratory for Hydrospheric Processes
NASA Goddard Space Flight Center

National Aeronautics and
Space Administration

Goddard Space Flight Center
Greenbelt, Maryland 20771

September 2000

Acknowledgments

This paper was not possible without the development of the Poseidon GCM by Paul Schopf, George Mason University Center for Ocean-Land-Atmospheres, and the provision of code for integration. Michele Rienecker, NASA/GSFC, provided meaningful insight into the GCM results and dynamics. The NASA/Goddard Space Flight Center Distributed Active Archive Center provided the CZCS data that was used for comparison. Margarita E. Conkright (NODC/OCL) provided *in situ* nitrate seasonal climatologies. This work was supported under NASA Grant (RTOP) 971-622-51-31.

Available from:

NASA Center for AeroSpace Information
7121 Standard Drive
Hanover, MD 21076–1320
Price Code: A17

National Technical Information Service
5285 Port Royal Road
Springfield, VA 22161
Price Code: A10

TABLE OF CONTENTS

ABSTRACT

A coupled ocean general circulation, biogeochemical, and radiative model was constructed to evaluate and understand the nature of seasonal variability of chlorophyll and nutrients in the global oceans. Biogeochemical processes in the model are determined from the influences of circulation and turbulence dynamics, irradiance availability, and the interactions among three functional phytoplankton groups (diatoms, chlorophytes, and picoplankton) and three nutrients (nitrate, ammonium, and silicate).

Basin scale (>1000 km) model chlorophyll results are in overall agreement with CZCS pigments in many global regions. Seasonal variability observed in the CZCS is also represented in the model. Synoptic scale (100-1000 km) comparisons of imagery are generally in conformance although occasional departures are apparent. Model nitrate distributions agree with *in situ* data, including seasonal dynamics, except for the equatorial Atlantic. The overall agreement of the model with satellite and *in situ* data sources indicates that the model dynamics offer a reasonably realistic simulation of phytoplankton and nutrient dynamics on synoptic scales. This is especially true given that initial conditions are homogenous chlorophyll fields.

The success of the model in producing a reasonable representation of chlorophyll and nutrient distributions and seasonal variability in the global oceans is attributed to the application of a generalized, processes-driven approach as opposed to regional parameterization and the existence of multiple phytoplankton groups with different physiological and physical properties. These factors enable the model to simultaneously represent many aspects of the great diversity of physical, biological, chemical, and radiative environments encountered in the global oceans.

1. INTRODUCTION

The seasonal cycle is one of the dominant signals in global ocean chlorophyll and nutrient distributions. Although solar radiation and the time-lagged heat cycle are ultimately responsible for the seasonal cycle, a complex set of physical, biological, chemical, and radiative processes determine the nature of the variability. A complete observation of these processes and their interactions on a global scale is beyond our capabilities because of the vast expanse of the oceans, despite the advent of routine spaceborne observational programs.

It is a challenge to represent the wide diversity of the global oceans. Other attempts, e.g. Longhurst (1995); Sathyendranath et al. (1995); Platt et al. (1991), subdivided the oceans into functional regions or provinces. These provinces are distinguished from one another in several key physical, biological and chemical conditions. This type of analysis provides an excellent representation of the spatial diversity of global ecosystems and many of the underlying causes. However, the influences of dynamical processes, regional discontinuities, and interannual variability can cause difficulties.

Numerical models of fundamental processes offer an alternative method to identify and elucidate the specific causes, magnitudes, and nature of seasonal variability. Considerable success has been achieved using coupled three-dimensional representations of physics and biogeochemistry in the North Atlantic (Dutkiewicz et al., 2000; McGillicuddy et al., 1995a; Sarmiento et al., 1993; Fasham et al., 1993) and equatorial Pacific Oceans (Chai et al., 1996; Toggweiler and Carson, 1995). This effort builds on this previous work as well as efforts coupling three-dimensional physical, biological, chemical, and radiative processes in selected regions (e.g., Walsh et al., 1999; Gregg and Walsh, 1992) in an attempt to construct a reasonable representation of global chlorophyll and nutrient dynamics, the processes affecting them, and their seasonal variability.

In this coupled, interactive model of circulation, biological, chemical, and radiative processes, regional characterizations are avoided. This representation attempts to simulate the wide range of global phytoplankton abundances and diversity using common processes, that are modified by the characteristics of the prevailing physical environment. Thus the model is general. While this approach may result in some lack of accuracy in the final global representations, we gain an understanding of the fundamental processes producing the distributions of phytoplankton. Such a representation naturally leads to a reduction of parameterizations as well, and focuses the problem on the influence of processes.

Essentially, a generalized parameter is defined as that which is in agreement with the realm of typical ocean conditions. Naturally occurring processes are sought that affect that representation in different physical conditions, and then the environmental conditions are allowed to dictate the specific response. For example, we define a gross sinking rate according to a typical phytoplankton diameter and under typical temperatures and viscosities using Stokes Law. Then sinking rates are allowed to vary according to the different viscosities encountered in the global ocean. Similarly, phytoplankton growth and herbivore grazing responses are based on temperature, photoadaptation and carbon:Chlorophyll states are based on irradiance in the water column.

In summary, the key features of the coupled model are:

1) Global scale, three-dimensional, with interactive and general hydrodynamical, biological, chemical, and radiative transfer processes

2) Multiple phytoplankton groups, which differ in growth rates, sinking rates, and optical properties

3) No regional tuning – the model uses explicit common global processes

Since seasonal variability is the focus of the present effort, a climatological representation of atmospheric and oceanic forcing conditions is employed. Results are compared to observations where available. The focus here is on the surface layer only because of the availability of remote sensing data for validation. Additionally, this paper emphasizes the coupling between the circulation and biogeochemical components of the model, and the radiative model is only briefly described. Further analysis of the interactions of the radiative coupling are discussed elsewhere (Gregg, 2000).

2. METHODS

This effort assumes that, in first order, the large scale (synoptic scale; 100-1000 km) and low frequency (subtidal) features of global, seasonal, and biogeochemical distributions may be described by a system of equations comprising mixing, advection, sinking, and growth of phytoplankton as a function of light, temperature, and nutrient availability and death by ingestion and senescence. This assumption leads to a set of coupled, partial differential equations called the governing equations of the simulation analysis

$$\frac{\partial}{\partial t} C_i = \nabla(A\nabla C_i) - \nabla\bullet\mathbf{V}C_i - \nabla\bullet(\mathbf{w}_s)_i C_i + \mu_i C_i - gH - sC_i \quad (1)$$

$$\frac{\partial}{\partial t} N_k = \nabla(A\nabla N_k) - \nabla\bullet\mathbf{V}N_k - b_k\Sigma_i C_i\mu_i + [b_k\gamma_k g\Sigma_i C_i]H + b_k\varepsilon_k s\Sigma_i C_i + b_k\varepsilon_k[n_1 H + n_2 H^2] + b_k r_k D \quad (2)$$

$$\frac{\partial}{\partial t} H = \nabla(A\nabla H) - \nabla\bullet\mathbf{V}H + [\Sigma_k(1-\gamma_k)g\Sigma_i C_i]H - n_1 H - n_2 H^2 \quad (3)$$

$$\frac{\partial}{\partial t} D = -\nabla\bullet\mathbf{w}_d D - \Sigma_k r_k D + \Sigma_k(1-\varepsilon_k)s\Sigma_i C_i + \Sigma_k(1-\varepsilon_k)[n_1 H + n_2 H^2] \quad (4)$$

where the subscripts k and i denote the existence of discrete quantities of nutrients (N, as nitrate, ammonium, and silicate) and chlorophyll (C, as diatoms, chlorophytes, and picoplankton), and bold denotes a vector quantity. H represents herbivores and D represents detritus. Other symbols are defined in Table 1.

The first term on the right hand side in Eqs. 1 and 2 represents diffusion, the second represents advection. The third in Eq. 1 only is sinking (which does not apply to dissolved nutrients, and also goes to zero in the horizontal), and the remaining terms are the biological processes terms. Explicit advection and diffusion processes are ignored for detritus to reduce the computational burden. However, advection and diffusion processes become represented when detritus remineralizes back to nutrient form (Eq. 2).

To solve this set of equations, one requires three separate models to obtain numerical values for the variables. A circulation model computes advection, mixing, and sinking and thus determines the time-dependent horizontal and vertical motions of phytoplankton, nutrients, herbivores, and detritus. A biogeochemical processes model derives growth of phytoplankton resulting from the calculated light field, temperature, and nutrient assimilation and death resulting from grazing and other ingestion as well as senescence. It also determines the fate of nutrients, herbivores, and detritus as related to the growth and abundance of chlorophyll. The radiative model determines the availability of light at the surface and in the water column. A diagrammatic representation of the fully coupled dynamic model illustrates the interactions among the three major components: a global hydrodynamical General Circulation Model (GCM), a general biogeochemical processes model, and a general radiative model (Figure 1). Although there are several nominal outputs of the coupled model, e.g., spectral radiance, primary production, and biogeochemical constituent distributions, only the latter are considered here.

Table 1. Notation for governing equations and general parameters. Values are provided for the parameters and ranges are provided for the variables.

Symbol	Meaning	Value	Units
A	Diffusivity	Variable	$m^2\ s^{-1}$
∇	Gradient operator	none	none
$\mathbf{V}$	Vector velocity	Variable	$m\ s^{-1}$
$\mathbf{w}_s$	Vector sinking rate of phytoplankton	0.0035-1.2	$m\ d^{-1}$
$\mathbf{w}_d$	Vector sinking rate of detritus	2.0	$m\ d^{-1}$
μ	Specific growth rate of phytoplankton	0-2	d^{-1}
g	Grazing rate by herbivores	0-2.15	d^{-1}
s	Senescence	0.05	d^{-1}
b	Nutrient/chlorophyll ratio	25 - 80	$\mu M\ (\mu g\ l^{-1})^{-1}$
n_1,n_2	Heterotrophic loss rates	0.1,0.5	d^{-1}
r	Remineralization rate	0-0.008	d^{-1}
ε	Nutrient regeneration by senescence	0.25	d^{-1}
γ	Herbivore grazing efficiency	0.25	d^{-1}
R_m	Maximum grazing rate at 20° C	1.0	d^{-1}
R	Maximum grazing rate	0.48-2.15	d^{-1}
Λ	Ivlev constant	1.0	$(\mu M)^{-1}$
K_N	Half-saturation constant (nitrogen)	1.0	μM
K_S	Half-saturation constant (silica)	0.2	μM

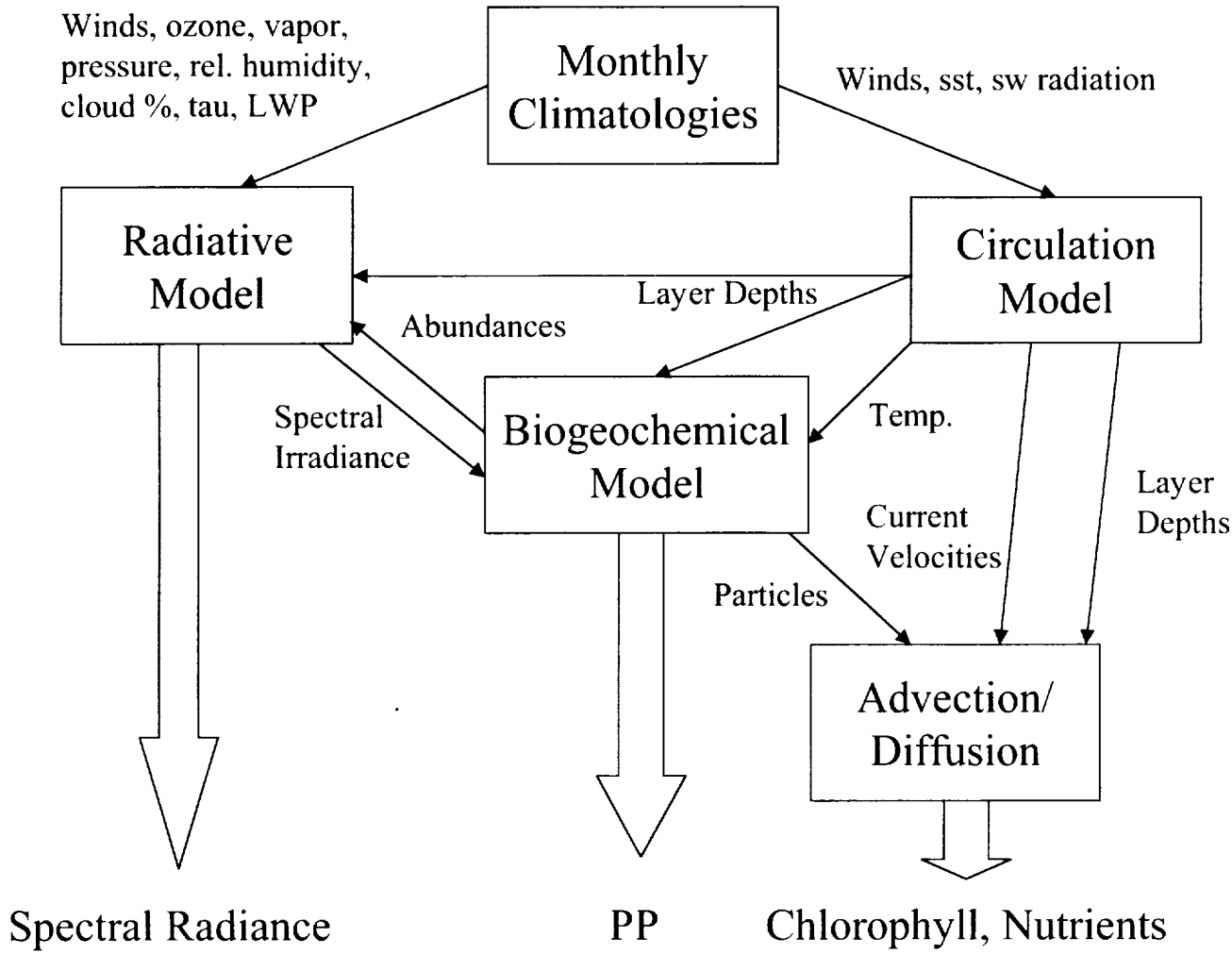

Figure 1. Diagrammatic representation of the coupled circulation, biogeochemical, and radiative model of the global oceans. Monthly climatological wind and atmospheric optical properties are used to drive the surface forcing. The hydrodynamics are affected directly through the wind stress and indirectly through the conversion of irradiance energy to heat in the radiative transfer model. The radiative model affects the biogeochemical model by determining the amount of total spectral irradiance available for growth of phytoplankton. Nutrient availability and herbivore ingestion also regulate phytoplankton populations locally. Outputs from the model are spectral upwelling radiance, primary production (which is an explicit calculation derived from the growth functions), chlorophyll abundances for each of the phytoplankton groups, and nutrients (nitrate, ammonium, and silicate).

2.1 General Circulation Model

The GCM is a reduced gravity representation of circulation fields and is nearly global in scale, extending from near the South Pole to 72° N, in increments of 2/3° latitude and 1 1/4° longitude (Schopf and Loughe, 1995). Only ocean areas with depths exceeding 200 m are active. The model contains multiple vertical layers, in quasi-isopycnal coordinates, with the deepest interface in the model at a mean depth of 2800 meters. The number of layers is a choice between vertical resolution and computational expense. A 14-layer version provides an adequate representation of surface and upper ocean hydrodynamics at reasonable computational cost. The surface layer represents the upper mixed layer, then there are several layers of fixed thickness to prevent outcropping, and the remaining layer depths are based on the density distribution. The water beneath the deepest interface is assumed to sustain no pressure gradients (i.e., a reduced gravity approximation).Vertical mixing is Richardson number-dependent, following Pacanowski and Philander (1981), and is performed in a time splitting mode, occurring every 12 h in contrast to the 0.5 h Δt of the advective processes. Experiments at shorter Δt (6 h) indicated little discernible effect. When vertical instabilities occur, convection results and is parameterized as vertical mixing at a large diffusion coefficient. The model uses a midpoint leap frog method to advance in time (Roache, 1982) and is driven by monthly climatologies of wind stresses, heat fluxes, and sea surface temperature (da Silva, 1994). The surface layer temperature of the model relaxes to sea surface temperature computed daily. The model is initialized by temperature and salinity from annual climatologies (Levitus and Boyer, 1994; Levitus, et al., 1994) and run for 5 years to achieve steady state.

2.2 General Biogeochemical Model

The biogeochemical model utilizes the circulation fields and the vertical mixing processes to produce horizontal and vertical distributions of constituents. The biogeochemical constituents have their own local dynamical processes (Figure 2). There are 3 phytoplankton groups: diatoms, chlorophytes, and picoplankton, which differ in maximum growth rates, sinking rates, nutrient requirements, and optical properties to help us represent the extreme variety of physical environments encountered in a global model (Figure 3). Picoplankton in this model are considered to be a group of very small prokaryotic plankton comprised mostly of cyanobacteria but including prochlorophytes. Three nutrients are included to simulate "new" use of nitrogen (Dugdale and Goering, 1967; Eppley and Peterson, 1979) represented by nitrate, regenerated nitrogen represented by ammonium, and silicate as an additional requirement of diatoms. Phytoplankton are ingested by a separate herbivore component, which also contributes to the ammonium field through excretion. Death by senescence contributes a small portion to the ammonium pool but mostly to the detrital pool, which is ultimately remineralized back to original nutrients. The biogeochemical model has 8 state variables in the fully coupled model.

Phytoplankton growth is a function of light and nutrient availability and temperature. It is evaluated at the minimum value for light and nutrients to represent the effects of a single limiting factor (Pribble et al. 1994) rather than multiplicative factors (e.g., Gregg and Walsh, 1992) and adjusted by temperature

$$\mu = \min[\mu(E_l), \mu(NO_3), \mu(NH_4), \mu(SiO_3)]\, \mu(T) \qquad (5)$$

where μ is the total specific growth rate (d^{-1}) of phytoplankton, E_l is the total irradiance (μM quanta m^{-2} s^{-1}), and NO_3, NH_4, and SiO_3 are the nitrate, ammonium, and silicate concentrations, respectively (μM). The total specific growth rate is modified by temperature according to Eppley (1972)

$$\mu(T)_i = (0.851\alpha\ 1.066^T)\beta_i \qquad (6)$$

where α is a factor to convert to units of d^{-1} (instead of doublings d^{-1}) and to adjust for a 12-hour photoperiod, and β is an additional adjustment used for the picoplankton component that reduces their growth rate in cold water (<15 °C)

$$\beta_3 = 0.0294T + 0.558 \qquad (7)$$

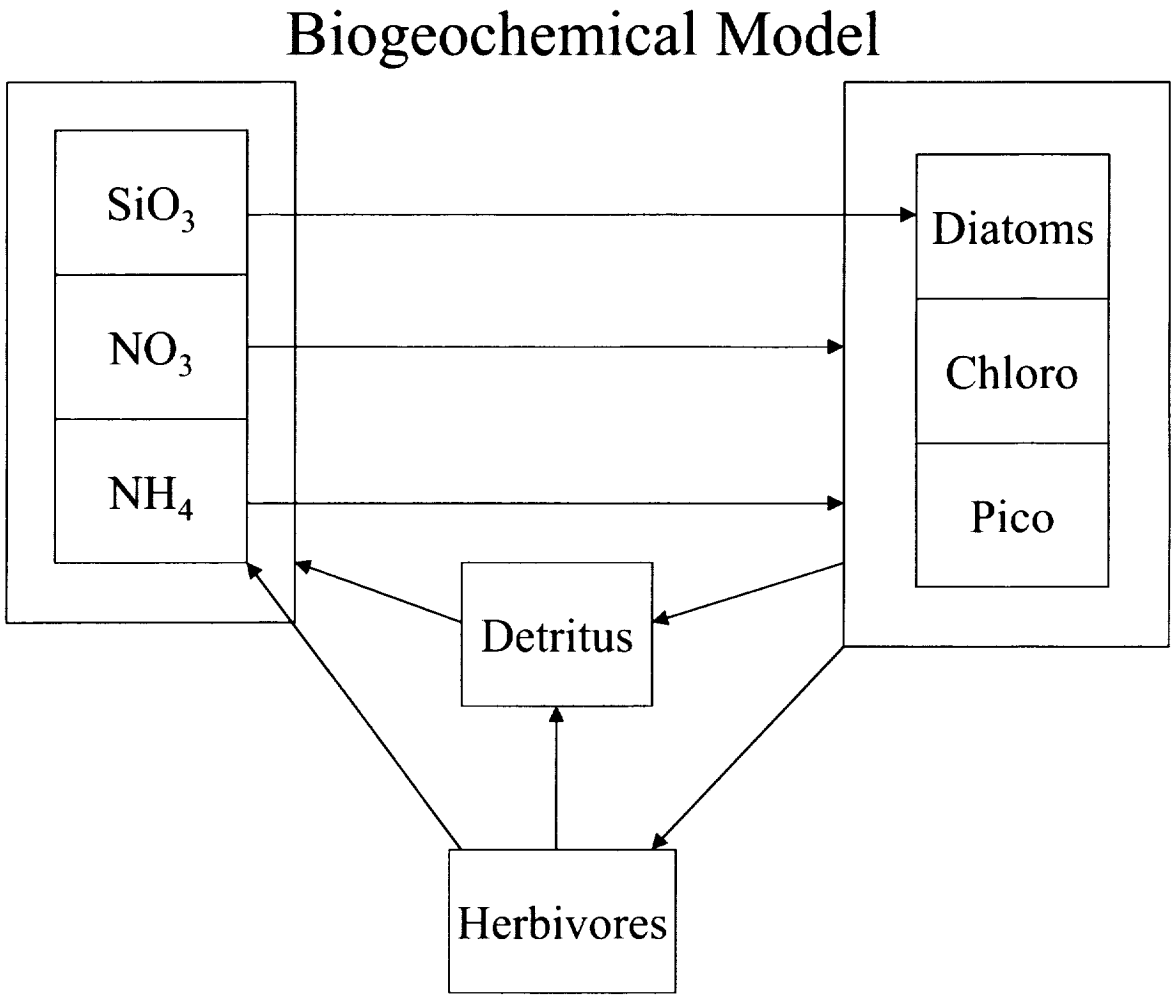

Figure 2. Diagrammatic representation of the biogeochemical model. Three phytoplankton components (diatoms, chlorophytes and a generalized picoplankton group representing prokaryotic plankton) interact with three nutrient components (nitrate, ammonium, and silicate) and, when ingested or upon death, contribute to detritus which returns to the ammonium pool immediately and the nitrate pool later upon remineralization. Herbivores ingest phytoplankton groups non-preferentially and contribute to the ammonium pool though excretion and eventually the nitrate pool upon death and remineralization.

This effect produces a nearly constant Δmaximum growth rate with diatoms at low temperatures. Temperature effects are evaluated once per day for computational convenience.

Phytoplankton growth as a function of light is approximated using Kiefer and Mitchell (1983)

$$\mu(E_t) \frac{\mu_m E_t}{(E_t + K_E)} \quad (8)$$

where μ_m indicates the maximum growth rate, and K_E is the irradiance at which $\mu = 1/2\mu_m$. K_E is related to the commonly reported light saturation parameter, I_k, by the factor 0.5. Respiration is ignored in this model. Expressions for μm and K_E are phytoplankton group-dependent, and thus contribute to the overall group characterizations (Figure 3). K_E is additionally dependent on the prevailing irradiance to simulate photoadaptation. We divide photoadaptation into 3 classes: 50, 150 and 200 (μM quanta m^{-2} s^{-1}). We compute the mean irradiance during daylight hours and then classify the phytoplankton photoadaptive state accordingly. This calculation is only performed once per day to simulate a delayed photoadaptation response.

Correspondingly, carbon:chlorophyll ratios are related directly to the photoadaptation state. This simulates the behavior of phytoplankton to preferentially synthesize chlorophyll in low light conditions and to enable more efficient photon capture. These three C:chl states are 25, 50 and 80. The C:chl classification is important for evaluating primary production but, more immediately, for determining the nutrient:chlorophyll ratios which are computed assuming the Redfield elemental balances

$$b = (C:chl)/79.5 \quad (9)$$

Growth limitation is also nutrient-dependent, and follows the Monod uptake kinetics model. All phytoplankton groups are limited by nitrogen, as nitrate and ammonium, and diatoms are additionally limited by silicate concentrations. Ammonium is preferentially utilized over nitrate, following the formulation of Gregg and Walsh (1992). Half-saturation constants are group-independent (Table 1). The picoplankton component possesses a modest ability to fix nitrogen from the water column as is observed in the cyanobacterium *Trichodesmium* spp. (Carpenter and Romans, 1991). The nitrogen fixation is expressed as 0.001 the light-limited growth rate and only applies when nitrate availability is < 1 μM. The fixed nitrogen is denitrified by the detrital component to prevent nitrogen accumulation in the model domain.

Typical sinking rates for the phytoplankton groups (Figure 3) are computed by declaring representative individual sizes and then using Stokes Law under typical oceanic conditions, e.g.,

$$w_s = \frac{2g(\rho_i - \rho)}{9\nu\rho} r^2 \quad (10)$$

where w_s is the sinking rate, g is gravitational acceleration, ρ_i is the density of the phytoplankton component, ρ is the density of seawater, ν is the viscosity of seawater, and r is the particle radius (Csanady, 1986). Modification of this rate can occur under circumstances deviating from the typical conditions, such as in extremely cold water where viscosities are large. Using Stokes Law, this effect is parameterized in terms of temperature, normalizing to the sinking rate at 20° C

$$w_s(T) = w_s(20)[0.451 + 0.0178T] \quad (11)$$

Simulation of grazing by the herbivore component is based on McGillicuddy et al. (1995b).

$$g(T) = R(T)[1-\exp(-\Lambda\Sigma C_i)] \quad (12)$$

A temperature-dependence in grazing is enforced,

$$R(T) = R_m 1.1A(T)/A(20°) \quad (13)$$

which is normalized by the rate at 20° C

$$R(T) = R_m 1.1A(T)/A(20°) \quad (14)$$

Again temperature effects are evaluated daily. Note the functional similarity between this expression and the phytoplankton growth rate dependence. This temperature-dependence in grazing enables growth and grazing to remain in approximate balance over the diversity of environments in the global oceans.

There are no refuge populations in the model (e.g., Bissett et al., 1999). Phytoplankton groups are allowed to become extinct if conditions to support their survival do not exist.

2.3 General Radiative Transfer Model

Rigorous radiative transfer calculations are necessary to provide the underwater irradiance fields to drive growth of the phytoplankton groups, accounting for the absorption of light by water and other optically active constituents. The model contains a treatment of the spectral and directional properties of radiative transfer in the oceans and explicitly accounts for clouds. It contains an optical characterization of atmospheric and in-water optical constituents. The atmospheric radiative model is based on the Gregg and Carder (1990) spectral model for clear skies and relies on Slingo (1989) for spectral cloud transmittance. It requires external monthly climatologies of cloud properties (cloud cover, optical thickness, and liquid water path), surface pressure, wind speeds, relative humidity, and precipitable water. Computations are made only for the spectral range 350-700 nm (photosynthetically available radiation or PAR) since the model is used to drive phytoplankton growth only and only every 2 h to provide diurnal variability at an acceptable computational cost.

Oceanic radiative properties are driven by water absorption and scattering, and the optical properties of the phytoplankton groups. Three irradiance paths are enabled: a downwelling direct path, a downwelling diffuse (scattered) path, and an upwelling diffuse path (Gregg, 1999). All oceanic radiative calculations include the spectral nature of the irradiance. The influences of the radiative model are not discussed in detail in the present paper, which focuses on the interactions among the biogeochemical components and the resulting distributions.

2.4 Model Initialization

The model is initialized with annual climatologies for nitrate and silicate from Conkright et al. (1994a). The remaining biological/chemical variables are set to constant values: 0.5 μM ammonium and 0.05 mg m^{-3} for each of the phytoplankton groups. The biogeochemical constituents approach steady state after 2 years, which provides one complete seasonal cycle in every region. All analyses in this paper are for the fourth year of simulation, which very nearly mirrors the third year (< 0.5% change in global surface layer nitrate and chlorophyll concentrations), suggesting that steady state has been reached.

Analyses emphasize comparisons with Coastal Zone Color Scanner (CZCS) pigment data, which at present are the only source of climatology, given the recentness of the Sea-viewing Wide Filed-of-view Sensor (SeaWiFS) and the abnormal conditions that have persisted since its launch (El Niño and La Niña). The comparisons are basin scale (> 1000 km) which exhibit the overall performance of the model and direct image-to-image comparisons which are used to evaluate synoptic scale (100-1000km) aspects of the model as compared to the CZCS. CZCS pigments were converted to chlorophyll using O'Reilly et al. (1998) for the basin-scale comparisons but were left as pigments for the synoptic scale (imagery) analyses. Regions are defined as in (Conkright et al., 1994b, 1998a): Antarctic is defined as southward of –40° latitude, the North Pacific and Atlantic Oceans are northward of 40°, and equatorial regions are bounded by –10° and 10°. Comparisons are also made of seasonal nitrate climatologies from the National Oceanographic Data Center (NODC)/Ocean Climate Laboratory (OCL) archives (Conkright et al., 1998b; 1998c; 1998d).

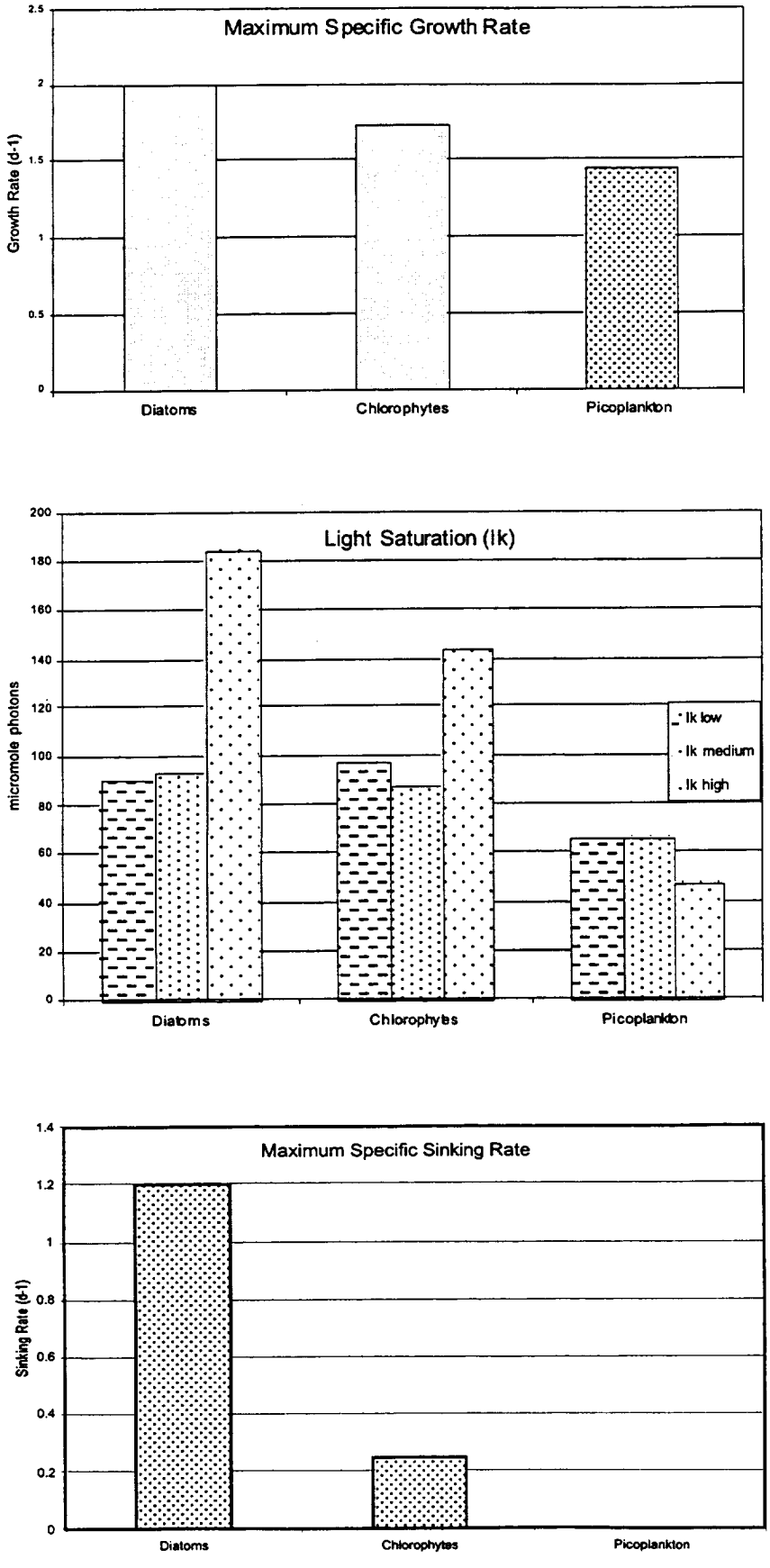

Figure 3. Phytoplankton group biological characteristics. Picoplankton characteristics are mostly from cyanobacteria but are intended to be generally representative of pico-prokaryotes. Values are means of reported data. Top: Maximum growth rate (from Brand et al. (1986; 1983); Furnas (1991); Gavis et al. (1981); Subba Rao (1981); Humphrey (1979); Ben-Amotz and Gilboa (1980); Eppley et al. (1969); Goldman and Glibert (1982). Middle: Light saturation parameters, I_k. Low light is defined as < 50 m moles photons m^{-2} s^{-1}, medium light is 50-200, and high light is > 200 (from Perry et al. (1981); Wyman and Fay (1986); Langdon (1987); Sakshaug and Andresen (1986); Bates and Platt (1984); Barlow and Alberte (1985). Bottom: Maximum sinking rates (derived from Stokes Law and representative phytoplankton sizes from Morel (1987); Bricaud and Morel (1986); Sathyendranath et al. (1987); Bricaud et al. (1983); Dubinsky and Berman (1986); Kirk (1975); Morel and Bricaud (1981); Mitchell and Kiefer (1988); Ahn et al. (1992); Bricaud et al. (1988). These figures illustrate the biological variety incorporated into the coupled model.

3. RESULTS AND DISCUSSION

3.1 Seasonal Trends in Chlorophyll: Basin Scale Means and Comparisons with CZCS

After 4 years from initialization, a regional basin scale comparison of the model-generated chlorophyll, with CZCS chlorophyll exhibits correspondence in seasonal cycles (Figures 4-6). The North Pacific and Atlantic show a pronounced spring bloom peaking near the boreal summer solstice (Figure 4). In the North Pacific, the magnitude of the bloom predicted by the model is larger than that observed by the CZCS but within the standard deviation. The timing and magnitude of the North Atlantic spring bloom is represented by the model. In both regions the CZCS indicates that the elevated chlorophyll biomass extends well into autumn while the model predicts a rather sharp die-off, especially in the North Pacific. The North Pacific actually indicates a boreal autumn bloom, that the model does not. In the model, these regions are characterized by large changes in surface mixed layer depth and a large variability in irradiance due to the seasonal variability in solar zenith angle and day length. This gives rise to mixed layer deepening in winter that, coupled with low irradiance, prevents significant phytoplankton growth. Turbulence and convective overturn provide nutrients to the surface layer that cannot be utilized. Upon the arrival of spring/summer, solar irradiance increases, and increased surface heating leads to shallower mixed layer depths. This provides the conditions for an extensive phytoplankton bloom, the dynamics of which are represented in the model. The late fall bloom in the CZCS, occurring in October-November, could be the result of mixed layer deepening and injection of nutrients but could also be due to poor sampling. Northerly portions of both the North Pacific and Atlantic are poorly sampled this time of year with the only sampling occurring in the southern portions of the basins. Since the low chlorophyll concentrations in the northern portions are underrepresented, the result is a biased mean chlorophyll. This is especially true in the North Atlantic. This is a major advantage of realistic numerical model simulations – the ability to produce estimates of chlorophyll under conditions precluding sampling from satellite such as low light levels. Still, sampled portions suggest higher values in the CZCS than produced by the model. Either death/ingestion/sinking losses are overestimated in the model for this time of year, or errors in the CZCS due to large solar zenith angles are occurring or a combination of both. Yoder et al. (1993) considered the CZCS data unreliable in fall and winter above 40° N.

The model exhibits agreement with the CZCS in the North Central Pacific and Atlantic gyres, with overall reduced abundances (mean chlorophyll near 0.1 mg m^{-3} compared to about 0.5 mg m^{-3} in the sub-polar regions; Figure 4). There is also the appearance of a late winter biomass maximum, occurring in early March. Both the model and CZCS exhibit generally elevated values in winter and depressed values in mid-to-late summer. The late winter maximum is produced in the model from mixed layer deepening (from 10m in August to about 75-100m in December/January) and injection of previously depleted nutrients into the surface layer where there is still sufficient irradiance to produce growth. However, due to a reduction in the average irradiance experienced by phytoplankton, the deep mixed layer prevents substantial growth. Shallowing of the mixed layer in spring leads to rapid depletion of available nutrients, and a decline in phytoplankton abundances throughout the summer.

Seasonal variability in the tropics is generally suppressed relative to other global regions (Figure 5). The maximum range of variability in the equatorial Indian, Pacific, and Atlantic oceans is only about 0.1 mg m^{-3}. This low range of seasonal variability is represented by the model. Even the small maxima and minima in the equatorial Indian and Atlantic Oceans appear to be in correspondence with CZCS chlorophyll. The seasonal variability of the North Indian in the model also appears to be in agreement with the CZCS, with maxima corresponding to the southwest monsoon in August and the less vigorous northeast monsoon in winter. However, the model appears to vastly underestimate the magnitude of the southwest monsoon, especially at the peak in August. The model also appears to underestimate the magnitude of the tropical Pacific chlorophyll concentrations.

The model appears to capture the strong seasonal signal in the North Indian Ocean/Arabian Sea region. However, the model is not as adept in matching magnitudes of the chlorophyll concentrations. The North Indian August mean chlorophyll in the CZCS is the single largest monthly mean recorded in any region in the entire CZCS record. Since it corresponds to the peak of the southwest monsoon, large chlorophyll concen-trations are expected here this time of year,

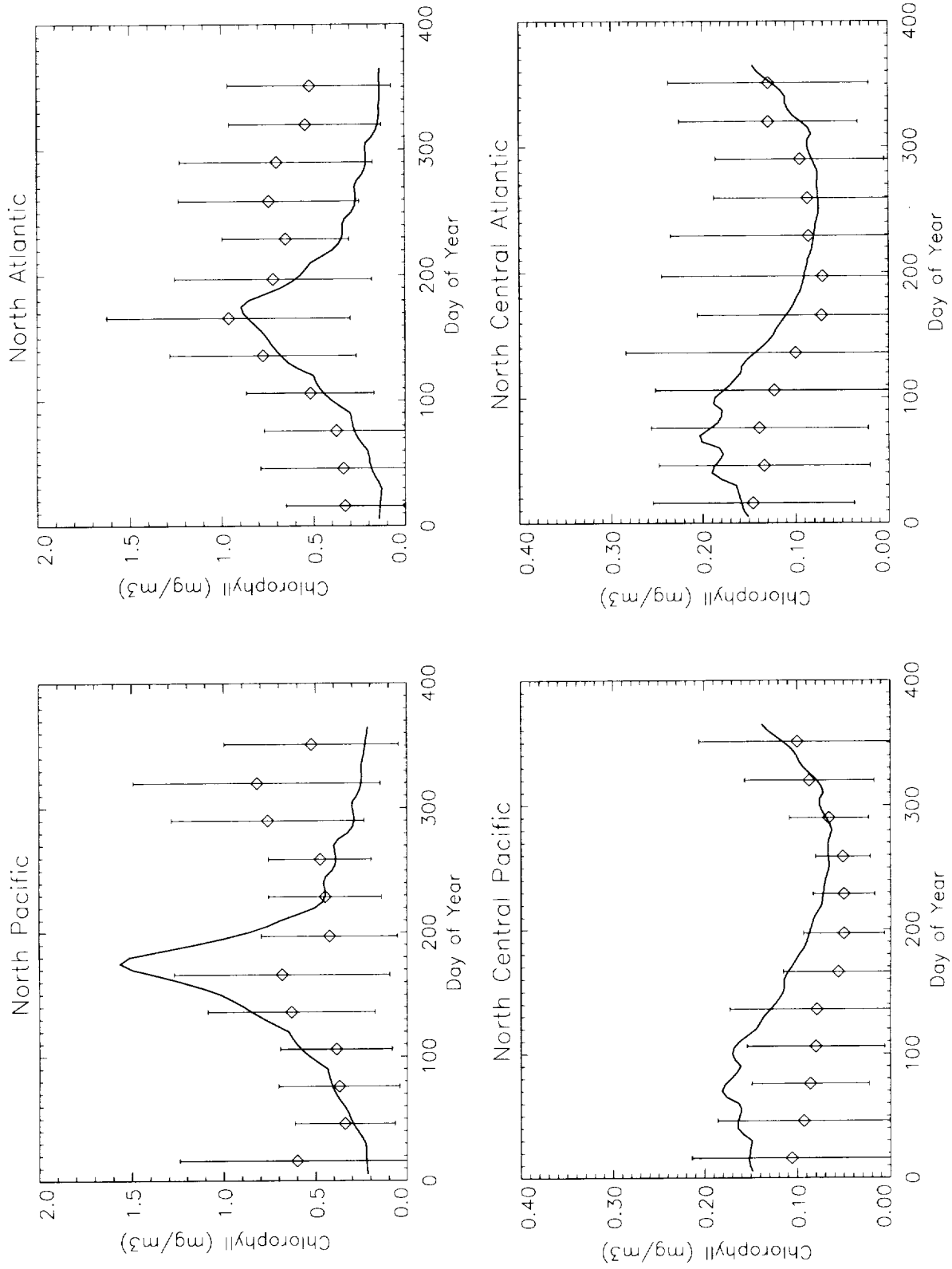

Figure 4. Comparison of model-generated mean chlorophyll (solid line) with climatological monthly mean CZCS chlorophyll in the Northern Hemisphere (open squares). Error bars on the CZCS chlorophyll represent one-half the CZCS standard deviation. Seasonal trends are in agreement although the magnitude of the spring bloom in the North Pacific appears to be overestimated by the model.

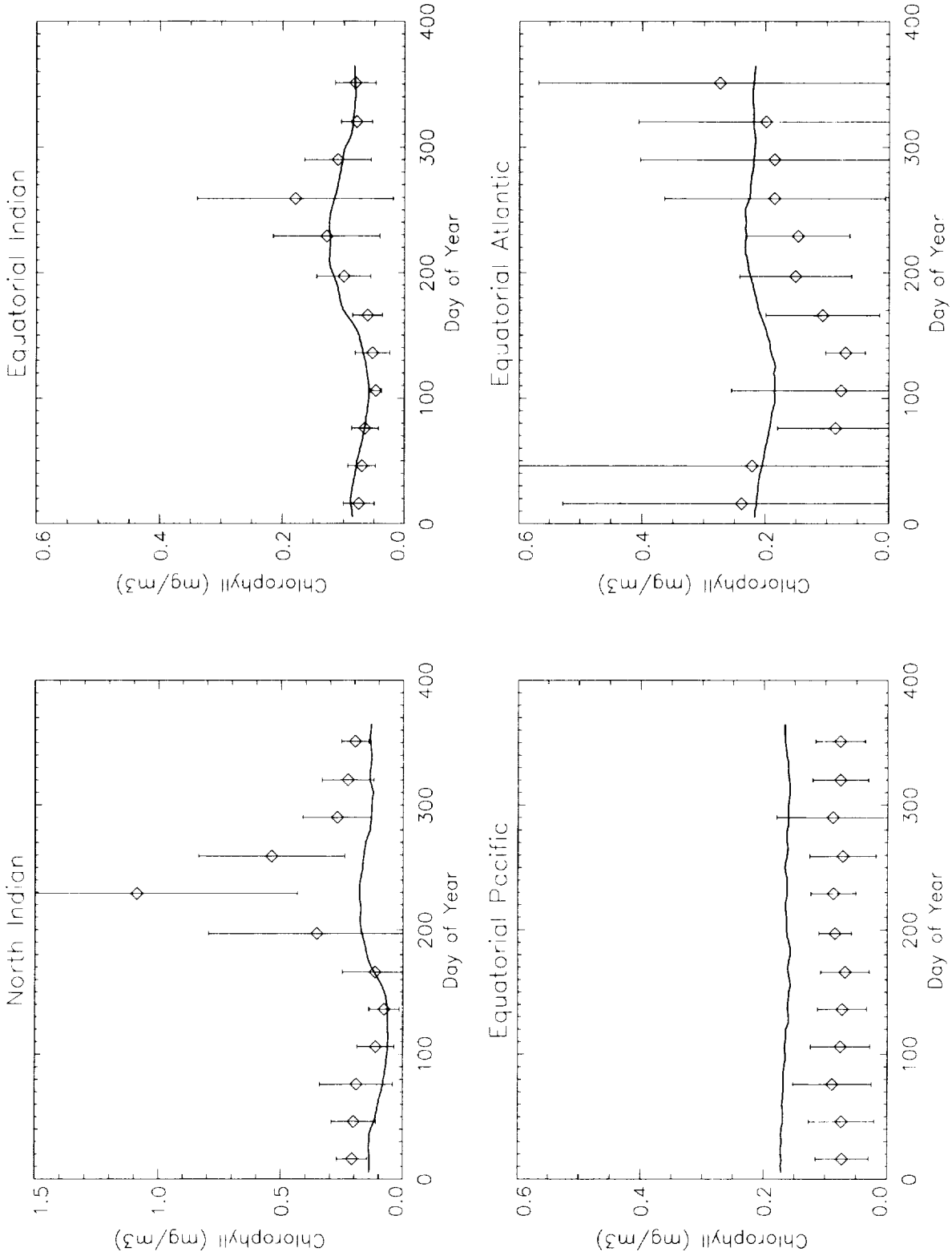

Figure 5. Comparison of model-generated mean chlorophyll (solid line) with climatological monthly mean CZCS chlorophyll in the tropics (open squares). Error bars on the CZCS chlorophyll represent one-half the CZCS standard deviation. Seasonal trends in all regions are represented by the model, but the magnitude of the southwest monsoon in the Arabian Sea appears to be vastly underestimated by the model.

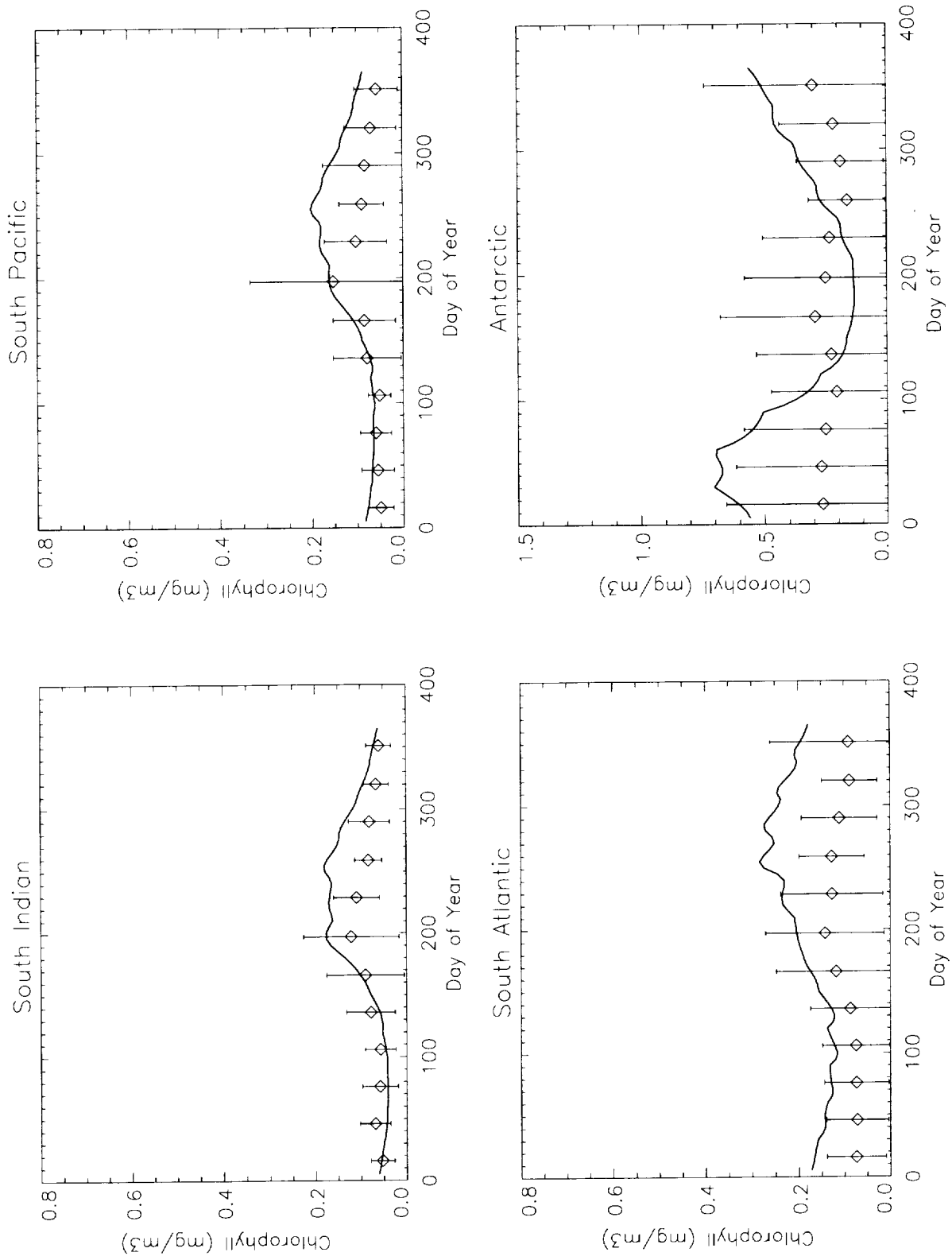

Figure 6. Comparison of model-generated mean chlorophyll (solid line) with climatological monthly mean CZCS chlorophyll in the Southern Hemisphere (open squares). Error bars on the CZCS chlorophyll represent one-half the CZCS standard deviation. Seasonal trends in all regions are represented by the model, except perhaps the South Atlantic.

Winds during this time of year can exceed 12 m s^{-1} as a monthly mean, which drives vigorous upwelling, nutrient availability, and associated phytoplankton growth. These dynamics are represented in the model, but associated with the strong winds is thick cloud cover (exceeding 80% as a monthly mean with cloud optical thickness of 4 or more), which in the model tends to suppress vigorous growth. The less vigorous northeast monsoon is also captured by the model (November-January) and is only slightly underestimated relative to the CZCS. Large concentrations of chlorophyll are observed from *in situ* records during the southwest monsoon (Conkright et al., 1998d), ranging from about 0.3 to 0.7 mg m^{-3} in the Arabian Sea. This is less than the CZCS but still greater than the model range of about 0.15 to 0.45 mg m^{-3}. The magnitudes that the CZCS observes (which exceed 3 mg m^{-3} over large parts of the Arabian Sea) may be suspect because of the presence of absorbing aerosols originating from nearby desert regions. These absorbing aerosols are incorrectly identified in the CZCS processing and thus will result in overestimates of chlorophyll if they are present.

Seasonal variability in the tropics is often smaller than the interannual signal, especially in the Pacific. The only significant seasonal influence is the motion of Inter-Tropical Convergence Zone (ITCZ), which is related to the sub-solar position. The model chlorophyll results reflect this lack of seasonal variability. However, the overestimate of tropical Pacific by the model is one of the most consistent trends in the comparison with CZCS chlorophyll. The model appears to represent the seasonal trends here (or lack of) but not the magnitudes. *In situ* chlorophyll data from the NODC/OCL archives suggest mean concentrations of between 0.1 and 0.2 mg m^{-3} (Conkright et al., 1998c), which is more in agreement with the model means (about 0.17 mg m^{-3}) and in contrast to the CZCS (which has a mean of about 0.07-0.08 mg m^{-3}).

In the Southern Hemisphere, again seasonal distributions of chlorophyll from the model are generally in agreement with CZCS in both timing and magnitude (Figure 6). The South Indian, Pacific, and Atlantic Oceans indicate a seasonal maximum occurring in mid-to-late austral winter (June-to-August). The model agrees with this trend except that the model predicts the elevated biomasses are sustained longer than the CZCS appears to indicate. In the South Atlantic, the maximum arises in the model about two months later than in the CZCS. Magnitudes in all three regions computed by the model are in agreement with the CZCS. The biomass peaks arise in the model due to mixed layer deepening occurring in the austral winter, similar to the processes described earlier for the North Central Pacific and Atlantic. Again the injection of nutrients into the mixed layer deepening is insufficient to allow profuse phytoplankton growth due to the depth of the layer itself, producing low irradiance availability experienced by the phytoplankton.

The Antarctic region is represented by the CZCS as virtually without seasonal variability, while in the model, it is a bloom-recede region similar to the northern Pacific and Atlantic, governed by the solar cycle and its influences on mixed layer depth and irradiance availability. Exceptionally poor sampling of this region by the CZCS during the austral winter almost certainly produces a bias such that the more northern portions of the region, where higher chlorophyll exists (and also in the model), are over-represented in the mean. Where there is sampling in the more southerly portions, the results suggest agreement of the model with the CZCS. However, when irradiance levels are more favorable for sampling, the CZCS chlorophyll data still do not exhibit a seasonal peak, while the model clearly indicates a summer bloom. Iron limitation would probably not eliminate the seasonal cycle, so it is unclear what is causing the disparity. This is one of the most poorly sampled regions by the CZCS, which may mask the seasonal cycle.

3.2 Seasonal Trends in Chlorophyll: Synoptic Scale Comparisons with CZCS

Imagery of simulated chlorophyll provides a better view of the nature and spatial distributions of the seasonal variability and how it compares to CZCS pigment. Four months are chosen to represent some of the range of seasonal variability exhibited by the model and observed in the CZCS (Figures 7 and 8). Generally, large-scale features are represented in the model and conform to CZCS data: vast areas of low chlorophyll in the mid-ocean gyres, elevated chlorophyll in the equatorial and coastal upwelling regions, and large concentrations in the sub-polar regions. The large scale features of the seasonal variability are represented as well: blooms of chlorophyll in local spring/summer in the high latitudes, followed by retreat in the local winter; expansion of low chlorophyll gyre regions in local summer, followed by contraction in winter; enhance-

ment in the Indian Ocean in August and December, and reduced concentrations in March and May. These features are evidence of realism in the model and its ability to simulate synoptic scale patterns and variability.

March represents a transition period when phytoplankton growth in the Southern Hemisphere is diminishing and growth in the Northern Hemisphere is accelerating (Figure 7). The beginning of the Northern Hemisphere spring bloom is apparent in both the model and the CZCS. The latitudinal extent is limited to about 50° N. In the model, this results from increasing day length and reduced solar zenith angles in the Northern Hemisphere and some mixed layer shallowing. Remnants of the Southern Hemisphere bloom are still apparent in CZCS imagery, especially near New Zealand, the Scotian Sea, and offshore of the Patagonian shelf. Patagonia is represented by the model, but the New Zealand area is underestimated, and the region of high chlorophyll in the Scotian Sea is displaced to the south. The model shows very low chlorophyll in proximity to the ice distribution, while the CZCS is somewhat higher although variable. Due to the presence of ice, it is likely that large pigment concentrations here in the CZCS are artifacts. Low chlorophyll concentrations near the ice sheets in the model are due to very cold temperatures, limiting the maximum growth rate. Coupled with continued sinking throughout the austral winter, phytoplankton populations become too small to sustain themselves for the duration of the non-growth season; this is in spite of reduced grazing accompanying the low temperatures. Here temperatures attain the model minimum of –2° C during the austral winter. The model requires a formulation of ice algal dynamics and austral spring melting and seeding in order to reasonably simulate this area. Such dynamics have been shown to be substantial contributors to the total primary production in these regions (Arrigo et al., 1997). Overall, the spatial variability of pigment distributions in CZCS is much larger than model chlorophyll. The model is driven by winds, sea surface temperatures, and cloud cover, which are apparently insufficient to capture the spatial variability apparent in the CZCS. In the search for reasons for the discrepancy, it may be due to the lack of circulation or mixing variability that is unavailable in the reduced gravity representation of the circulation model, the importance of eddy scale processes (McGillicuddy et al., 1998; Oschlies and Garcon, 1998), or that iron limitation is at work here (Martin et al., 1990).

The sub-polar transition zones in the South Atlantic, Indian, and Pacific Oceans are represented in the model, although the model exhibits generally larger concentrations and less spatial variability. In the model, the North Central Pacific gyre is smaller in size than in the CZCS, but the Southern Hemisphere mid-ocean gyres are almost matched. At this time of year, deep mixed layers with strong density interfaces are prevalent in the model in these regions in the model, suppressing phytoplankton growth by lack of nutrients and low average irradiance availability.

The tropical Pacific upwelling region has about twice the chlorophyll concentration in the model as in CZCS pigment, but the meridional and zonal extent is nearly the same (Figure 7). This suggests either excessive upwelling in the model or the lack of iron as a limiting nutrient in the model. This region is widely regarded as iron limited (Kolber et al., 1994; Coale et al., 1998). Although somewhat overestimated by the model in the Atlantic, tropical Atlantic and Indian Ocean features in CZCS pigment are represented in the model. Upwelling off the Mauritanian and Namibian coasts is represented in the model although with reduced peak values. The model underestimates the chlorophyll concentrations in the Arabian Sea and North Indian Ocean, but many of the same features are apparent. March corresponds to the inter-monsoon season here, but the season has not reached its maximum yet. A high concentration of chlorophyll off the coast of Costa Rica is apparent in both. This is strictly a boundary-induced upwelling feature in the model, but in the CZCS, it may be additionally influenced by the Coast Rica dome. The California coast exhibits strong upwelling in both the model and imagery.

In May the Northern Hemisphere spring bloom is in full swing in CZCS imagery and is apparent in the model (Figure 7). The northerly extent of the bloom extends to the edge of the model domain in the CZCS imagery and nearly so in the model. There is more spatial variability in the North Pacific in the CZCS than in the model, but the magnitudes and extent are similar. There are many specific features of the North Atlantic bloom that differ between the model and CZCS, but the overall structure and magnitude are similar. The model exhibits the result of increased solar heating, producing a shallow mixed layer replete with nutrients from the

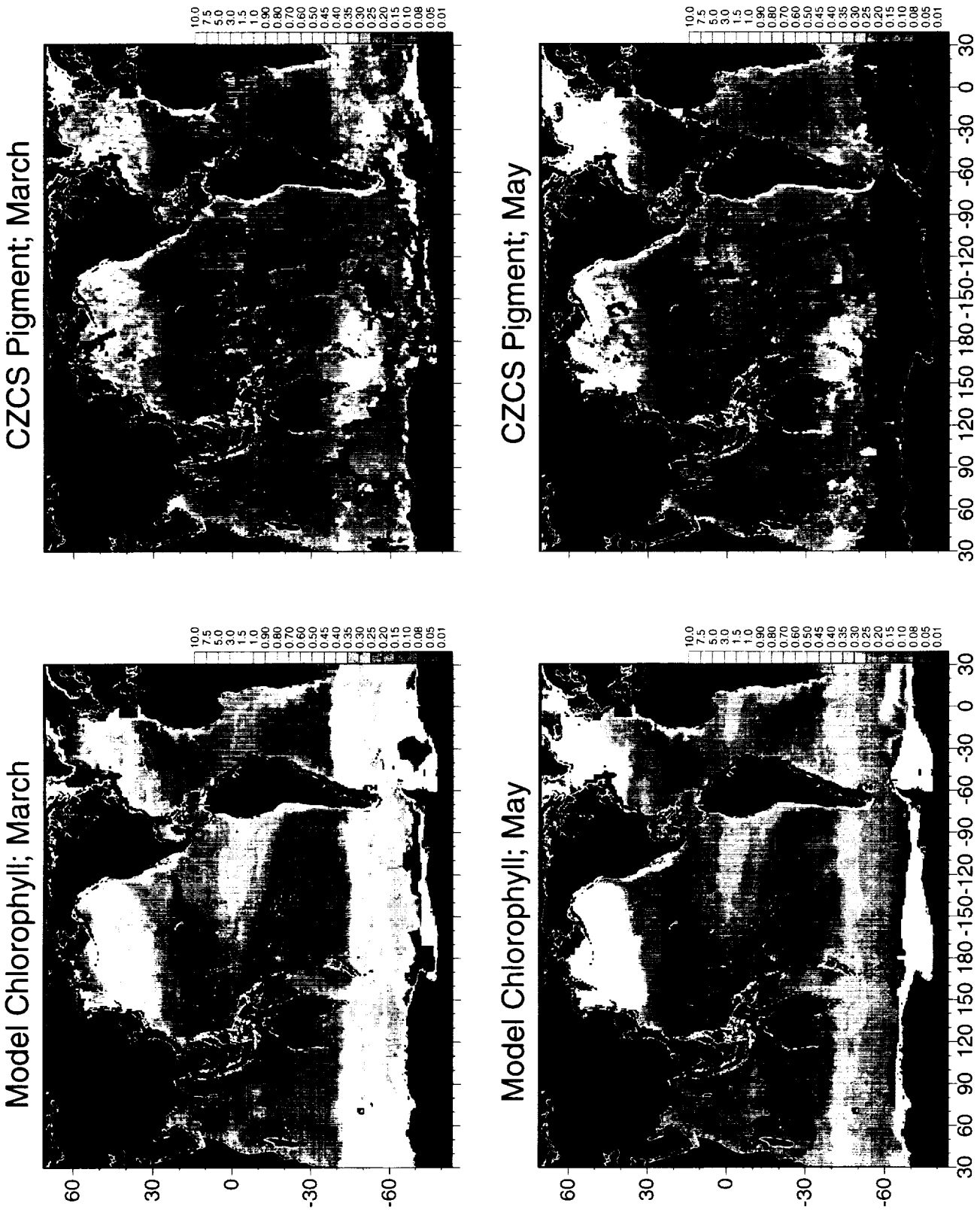

Figure 7. Model chlorophyll distributions for March and May (monthly means) and CZCS mean monthly pigment for the same months for comparison. Climatological monthly ice distributions are indicated, but are not part of the model computations. General features of chlorophyll distributions are in agreement.

long boreal winter, long days and small solar zenith angles to support phytoplankton growth and lagging zooplankton populations producing low grazing. Temperatures remain somewhat low to suppress the magnitude of the bloom which helps to produce the agreement with the CZCS.

In both the model and CZCS, the North Pacific and Atlantic gyres exhibit expansion from March. Because of only slightly larger values in the model at the periphery of the gyre in the Pacific (0.08-0.1 mg m^{-3} in the model compared to 0.04-0.08 mg m^{-3} in the CZCS), the shapes of the mid-ocean gyre regions do not conform. The North and equatorial Indian Oceans also have substantially reduced pigment concentrations. This is in agreement with the model, which is the result of the inter-monsoon season being fully underway with light winds, sluggish circulation patterns, and deep mixed layers.

The Southern Hemisphere gyres, in contrast to the Northern ones, exhibit contraction in May compared to March. This is true for both the model and CZCS, and sizes/magnitudes are represented in the model. The surface mixed layer is deepening in the model, entraining nutrients from below. The Patagonian and South Atlantic sub-polar transition zones are both diminished in chlorophyll relative to March, resulting in the model from larger solar zenith angles and shorter day length. These trends are represented in the CZCS. The Australia/New Zealand region of high pigment in CZCS is reduced in magnitude and extent in May, as it also is in the model, but again the model appears to underestimate the magnitude. The reduced gravity approximation and the lack of boundary effects originating from the nearby land (nutrient input) are possible explanations. Coverage south of –50° latitude is sparse in the CZCS, and the model is the only source of data. Where CZCS data exist, they appear to be in agreement with the model. In August the extent of the high latitude high pigment regions in the North Pacific and Atlantic is reduced as the gyres have expanded (Figure 8). Both model and CZCS show similar patterns. In the model, magnitudes have fallen slightly due to mild nutrient limitation and large grazing but appear to be sustained in the CZCS. The model now exhibits high chlorophyll to the northern edge of the domain, as does the CZCS. This is due to the heat flux finally exerting influence in these northerly regions, coupled with nearly constant day and associated high solar zenith angles. A very large expansion of the Northern Hemisphere mid-ocean gyres has occurred in both the model and CZCS. In the model this is due to the reduction of mixed layer depths and nutrient exhaustion.

Large pigment biomasses are observed in the CZCS in the North Indian Ocean and Arabian Sea. As noted earlier, the August North Indian is the largest mean biomass observed by the CZCS in its entire history. Due to the intensification of the southwest monsoon, the model also shows major increases in chlorophyll concentrations. But the model is not nearly as dramatic. The CZCS indicates a very large area of pigment values >1 and often >3 mg m^{-3} in the Arabian Sea. During the late southwest monsoon, *Gardner et al.* (1999) reported maximum surface values of about 3 mg m^{-3}, which quickly dissipated to about 1.2 mg m^{-3} in two days. This represented a time series of three days. The dynamics are present to produce these high concentrations, but *in situ* data from the NODC/OCL archive indicate mean summer chlorophyll values not exceeding 0.3-0.7 in this area (Conkright et al., 1998d); this is more in agreement with the model. However, the *in situ* data represents a seasonal mean.

Enhancement of CZCS pigment in the tropical Atlantic is very strong in August as it also is in the model (Figure 8). The ITCZ is shifted northward, and, consequently, reduced cloud cover overlies the region. Due to upwelling in the model, large pigment concentrations are apparent in the CZCS along the Namibian coast. There is substantial contraction of the Southern Hemisphere gyres along with some modest enhancement of the Patagonian pigment. These patterns are represented by the model and are the result of mixed layer deepening and associated nutrient injection in the gyres and increased turbulent mixing in Patagonia. Compared to May, the observed portions of the Antarctic Ocean and sub-polar transition zones have larger mean pigment concentrations in the CZCS as well as in the model. One exception is the diminished pigment near New Zealand for which the opposite trend is found in the model. However, the net effect is to make the model basin-scale chlorophyll in better agreement with the CZCS this month. The model predicts very low biomasses south of –50° latitude. This is the result of very cold temperatures (< 0° C) and nearly constant darkness. CZCS data are either obscured by clouds or unsampled, but the slivers that exist (e.g., near 180° W) suggest some agreement with the model.

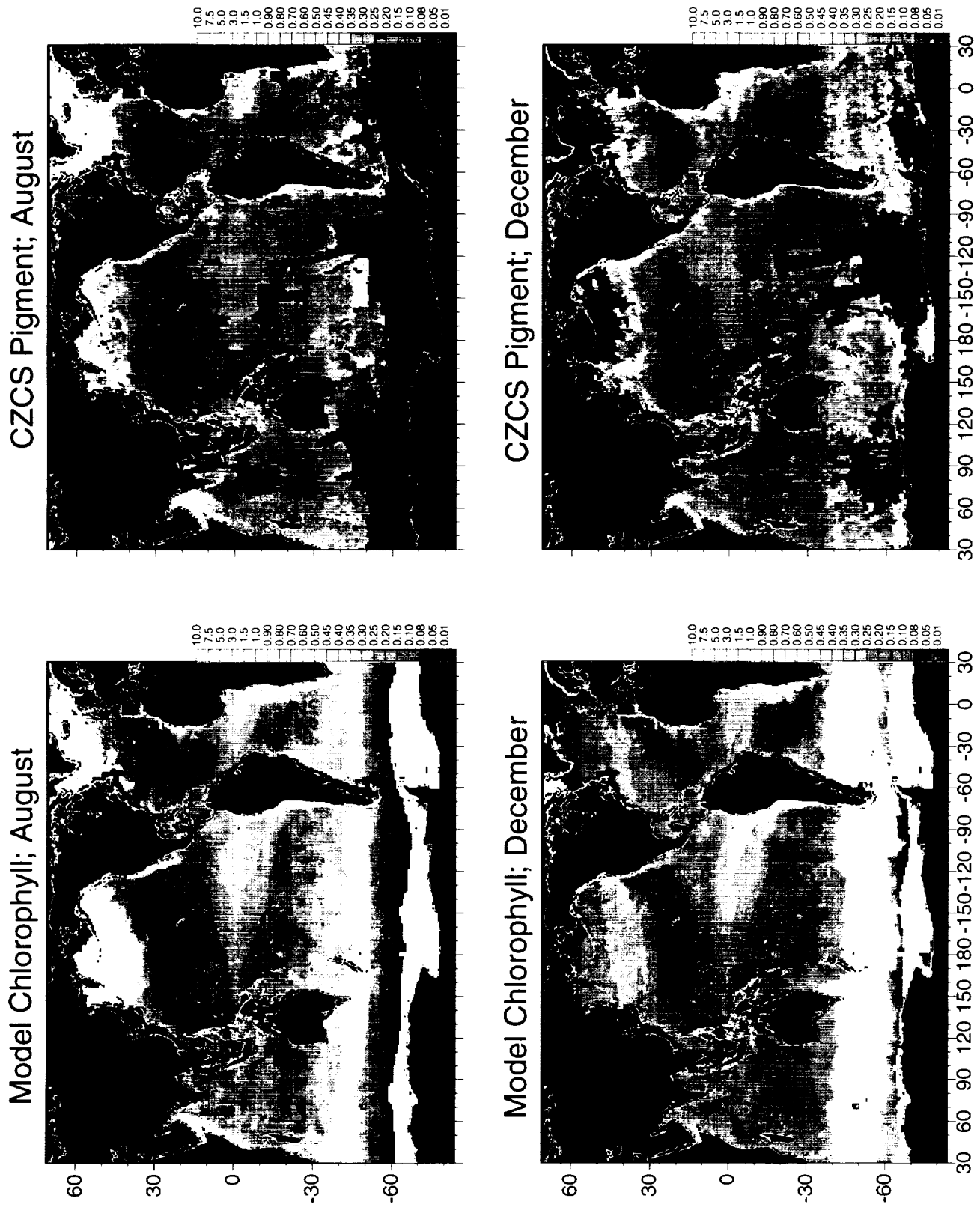

Figure 8. Model chlorophyll distributions for August and December (monthly means) and CZCS mean monthly pigment for the same months for comparison. Climatological monthly ice distributions are indicated, but are not part of the model computations.

December CZCS pigment concentrations illustrate a major reduction in magnitude in the northern sub-polar Pacific and Atlantic along with contraction of the Northern Hemisphere mid-ocean gyres as the sub-polar regions of high pigment have moved south (Figure 8). These trends are represented by the model. Along the western U.S. coast, there is intensification of pigment biomass in the CZCS that is not represented by the model. Again the model predicts larger chlorophyll concentrations in the tropical Pacific than in the CZCS, but the extent is matched. Note especially the area of high chlorophyll north of the main axis of the tropical upwelling located between 160° W and 100° W, which is also apparent in the CZCS. The tropical Atlantic shows intensification of pigment biomass in the CZCS from August, but the model shows a slight decrease in magnitude. A high concentration of chlorophyll off the coast of Namibia has grown in the model from August, while it has diminished in the CZCS. The tropical and North Indian Ocean and the Arabian Sea are reduced in chlorophyll in both the model and CZCS from August, but are still much larger than in May. Southern Hemisphere gyres begin to exhibit expansion from their distribution in August and the southern ocean is now increasing in chlorophyll and pigment. These trends are represented by the model, but the CZCS shows much greater spatial variability than the model.

3.3 Seasonal Trends in Nitrate: Synoptic Scale Comparisons with *In situ* Data

Model surface nitrate results are averaged over seasons and compared to *in situ* archives maintained by NODC/OCL (Conkright et al., 1998b; 1998c; 1998d). The results show overall agreement between the model and data, and features of seasonal variability are in conformance (Figures 9 and 10). Spatial distributions and magnitudes are represented by the model. Year-to-year nitrate differences in the model are < 0.5% by the beginning of the third year of simulation, suggesting that deep nitrate concentrations have equilibrated and are not influenced by the initial conditions. Two general exceptions to the overall agreement are the tropical Pacific and Atlantic. In both cases the model predicts much larger nitrate concentrations than are observed in the data. The departure is much reduced for summer and autumn in the Pacific, but the discrepancy in the Atlantic is persistent and large. *In situ* data show little apparent evidence of upwelling in the Atlantic, whereas the model exhibits strong upwelling. The CZCS pigments clearly show high biomasses indicative of upwelling (Figures 7 and 8). The conditions present, e.g., winds, coastal boundary, equatorial divergence, suggest upwelling, which is not supported by the *in situ* nitrate data. Large nitrate concentrations exist at 50-100 m in the *in situ* archive, suggesting immediate uptake by the phytoplankton as it advects/diffuses across the mixed layer.

Note how seasonal distributions of nitrate are represented in the North Pacific and Atlantic by the *in situ* data and the correspondence in model results (Figures 9 and 10). Large concentrations, with magnitudes and spatial extent matching the data are apparent in winter, but diminish in spring. By summer, magnitudes reach a minimum and begin to recover by autumn. In the model, large nitrate concentrations in the winter are due to lack of utilization by phytoplankton and availability through convective overturn in the boreal autumn and turbulent exchange. In boreal spring, nitrate concentrations begin to diminish due to nutrient utilization by phytoplankton in spring, when conditions supporting acceleration of growth are available (shallowing mixed layer and irradiance availability). By summer, the period of high phytoplankton growth has been occurring for several months, and little new exchange has occurred from deeper layers, resulting in severe reduction (but not depletion). The reduction of nitrate is much greater in the North Atlantic than in the Pacific. CZCS pigments suggest much larger biomasses in the N. Atlantic than Pacific, which would result in reduced nitrate concentrations in the Atlantic. The model, however, shows greater chlorophyll concentrations in the Pacific, which are due to the large availability of nitrate at the beginning of the growing season. Given that the nitrate concentrations appear to be reasonable in the model, this suggests that phytoplankton are limited in the North Pacific by some process or substance that is not explicit in the model. Again iron limitation is a possibility (Martin and Fitzwater, 1988). But more perplexing is the presence of large CZCS pigments in summer in the Atlantic associated with relatively low nitrate. By autumn, nitrate concentrations are beginning to be replenished as phytoplankton growth decreases from mixed layer deepening and reduced irradiance.

The Arabian Sea exhibits moderate nitrate values in winter, diminishing in spring, and attaining the maximum in summer. These trends are represented by

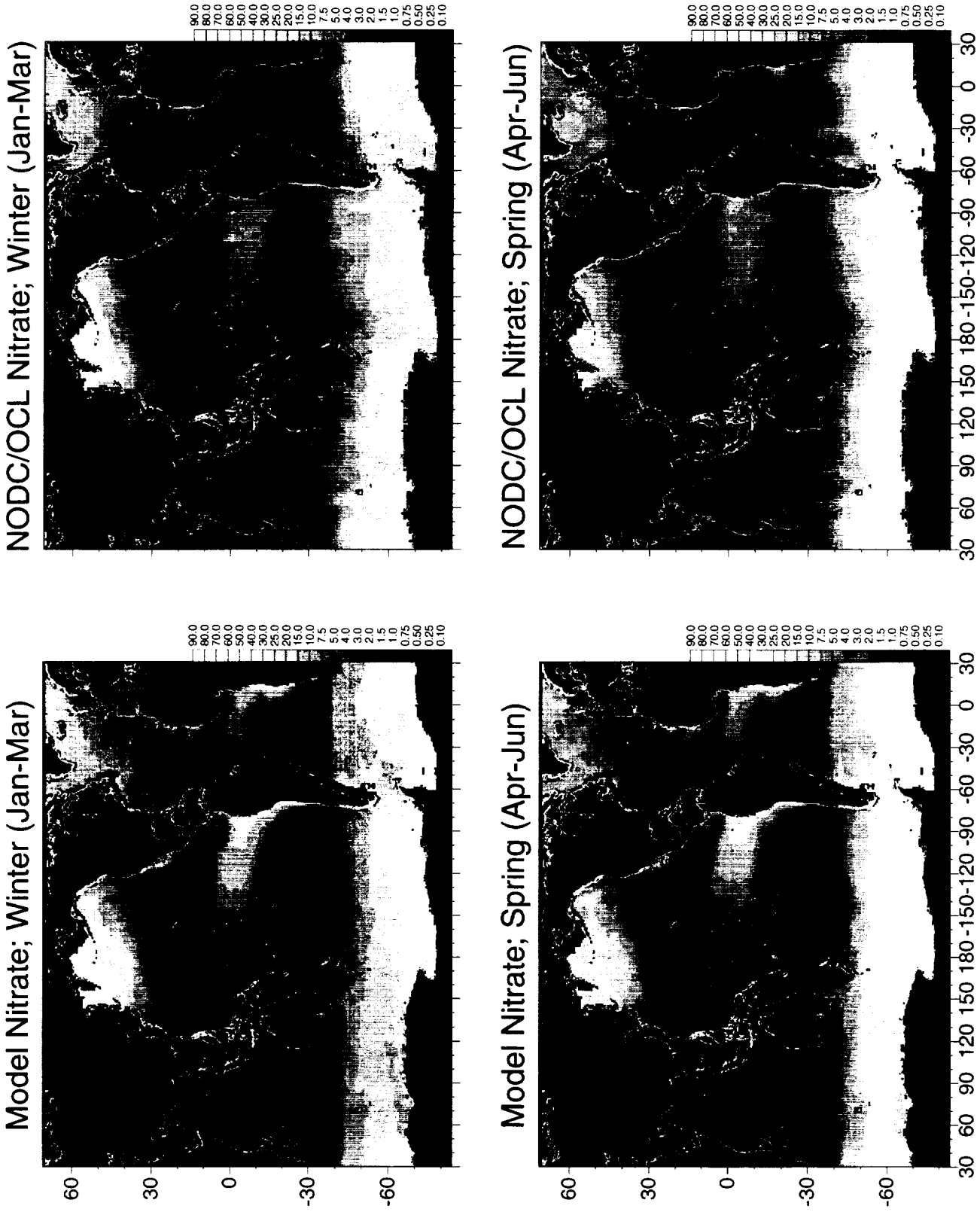

Figure 9. Comparison of model-computed surface nitrate distributions (averaged over seasons) with *in situ* data archives from NODC/OCL for winter and spring. Units are μM.

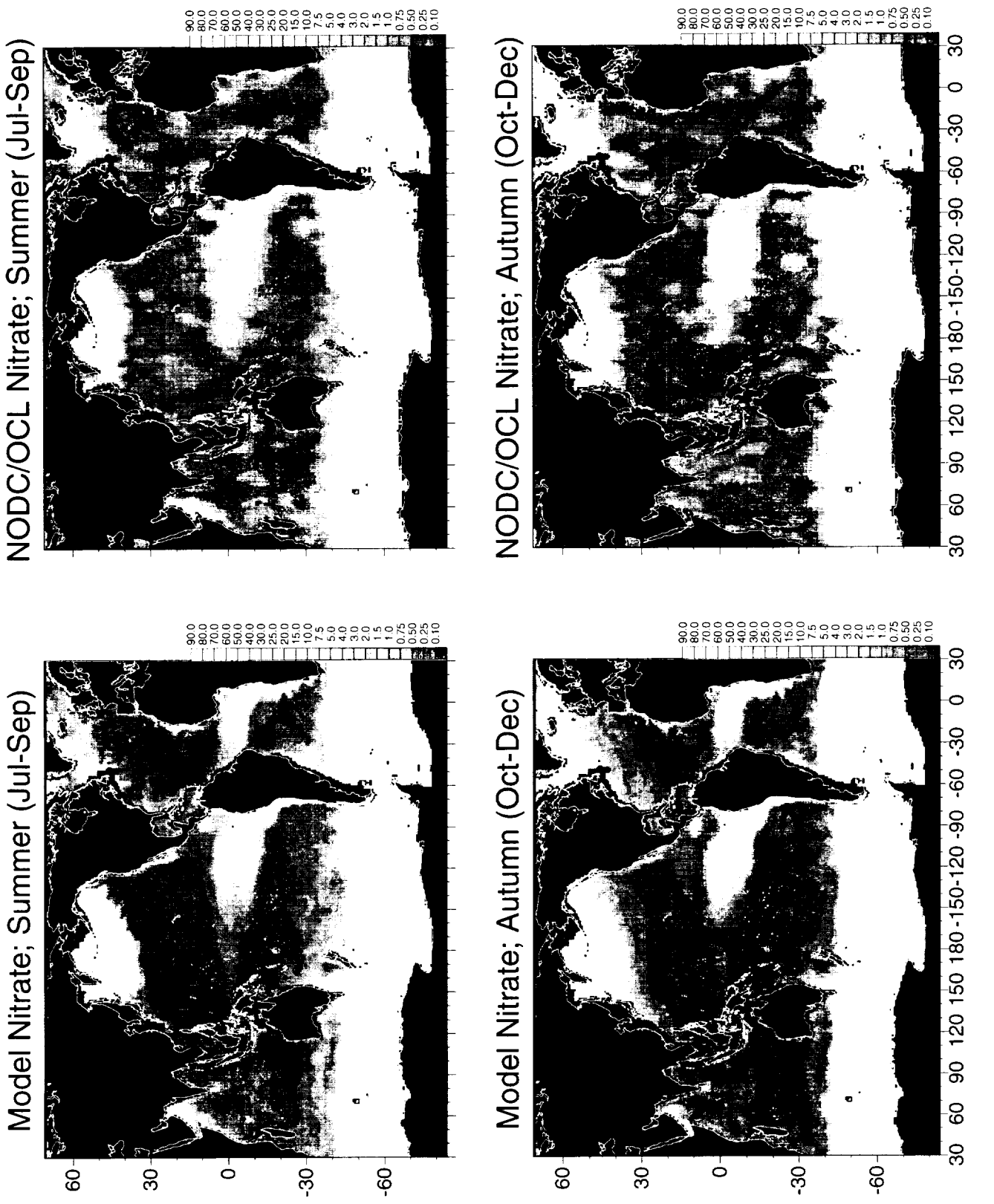

Figure 10. Comparison of model-computed surface nitrate distributions (averaged over seasons) with *in situ* data archives from NODC/OCL for summer and autumn. Units are μM.

the model, and are the direct result of circulation patters associated with the southwest and northeast monsoons, and the inter-monsoon periods.

3.4 Phytoplankton Group Distributions

Phytoplankton group distributions are initialized as equal values across the model domain (Figure 11). In April after 4 years of simulation, the three phytoplankton functional groups arrive at distributions that generally conform to expectations: diatoms predominate high latitude, coastal, and equatorial upwelling regions; picoplankton predominate the central ocean gyres; and chlorophytes inhabit transitional regions (Figure 12). The diversity of the functional groups and their different abilities to survive under different oceanic habitats is the main reason for the overall ability of the model to represent global chlorophyll patterns. Diatoms bloom first in the North Atlantic and the eastern North Pacific and predominate the Antarctic Ocean and sub-polar transition region. Eynaud et al. (1999) found that diatoms were predominant in the Antarctic Ocean but also found that coccolithophores predominated in the Antarctic sub-polar transition region. Chlorophytes predominate the western North Pacific and the edges of the equatorial upwelling regions outside the area that is dominated by diatoms. They also predominate at the edge of the sub-polar transition region in the south and have very large populations in the southern ocean from about 40° W eastward to 70° E. Picoplankton are generally distributed throughout the central gyres at low concentrations but have some larger abundances in the western North Pacific and Atlantic at the edge of the diatom blooms, in the southern periphery of the tropical Pacific upwelling, and offshore of Namibia. The predominance of picoplankton in the mid-ocean gyres is well-established (Glover, 1985; Itturiaga and Mitchell, 1986; Itturiaga and Marra, 1988).

In the model, diatoms follow the nutrients. Where there are abundant nutrient concentrations, diatoms tend to be prevalent. These regions occur in the model where kinetic energy is large: where convective overturn results in massive displacement of vertical water masses, where turbulent mixing processes are large, and upwelling circulation is vigorous. These are the high latitudes, coastal upwelling areas, equatorial upwelling areas, and regions of strong seasonal influences such as the Arabian Sea. This is because diatoms are the fastest growing of the functional groups contained in the model. This enables them to outcompete the other groups when nutrients and light are available. However, their large sinking rates prevent them from sustaining their populations in quiescent regions or periods. They require light and nutrients to produce growth rates that can enable them to sustain the large losses they incur from their sinking rates. These areas occur in the high kinetic energy regions of the global oceans.

Picoplankton are nearly the functional opposite of diatoms in the model. Slow growing and nearly neutrally buoyant, they cannot compete with diatoms under favorable growth conditions, but have a competitive advantage in low nutrient areas, by virtue of the low sinking rates and to a very minor extent their ability to fix molecular nitrogen. Thus, they predominate in quiescent regions, such as mid-ocean gyres, where kinetic energy is low, circulation is sluggish, mixed layer depths are deep, and nutrients are only occasionally injected into the mixed layer. While they are able to survive in these regions, the lack of nutrients and deep mixed layers produce an overall low average irradiance environment, and they never attain large concentrations. They occasionally attain some moderate concentrations, e.g., 0.25 mg m^{-3}, in isolated regions of the oceans. Some examples are the southern portion of the high chlorophyll regions in the north Pacific and Atlantic, the periphery of the tropical Pacific upwelling, and the periphery of the Benguela upwelling. Each case represents a transition zone from a high chlorophyll diatom-dominated region.

Chlorophytes generally represent a transitional group in the model, inhabiting areas where nutrient and light availability are insufficient to allow diatoms to predominate but not in areas where nutrients are so low to prevent losses by sinking to compensate by growth. This is a function of their intermediate growth and sinking rates relative to diatoms and picoplankton. Their largest concentrations tend to be at the transition between the diatoms and picoplankton, such as the southern edge of the northern spring bloom (vice versa for the southern bloom), or the edges of the tropical upwelling and Arabian Sea blooms. They are most responsible for the seasonal expansion/contraction of the mid-ocean gyres, which is one of the most significant seasonal signals in the model and in the CZCS record.

Since the North Pacific tend to predominate the western portion where one would expect diatoms to prevail, the North Pacific represents somewhat of an anomaly in chlorophyte distribution. This part of the

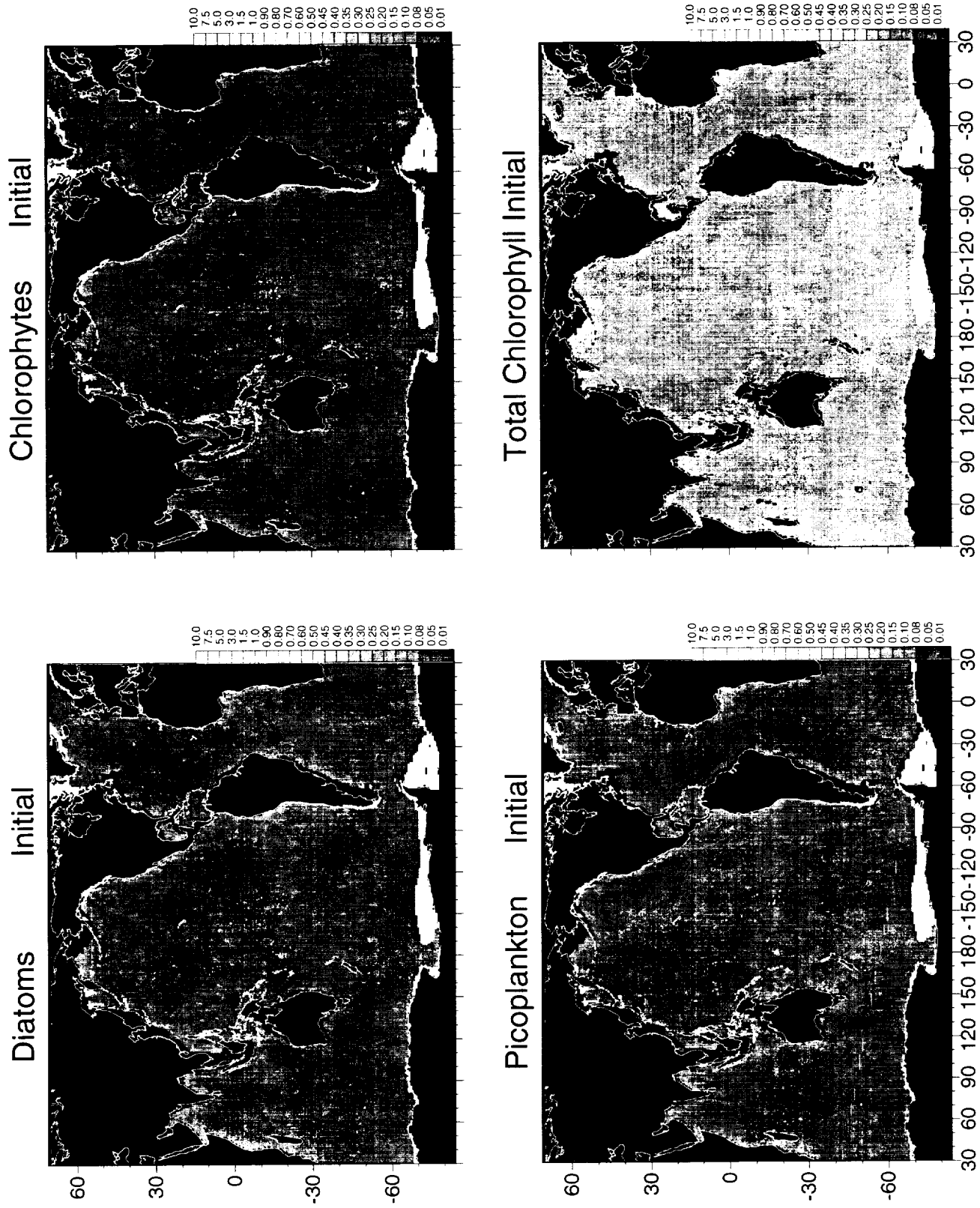

Figure 11. Initial surface conditions for the 3 functional phytoplankton groups in the coupled model (mg m^{-3}). Distributions with depth are the same.

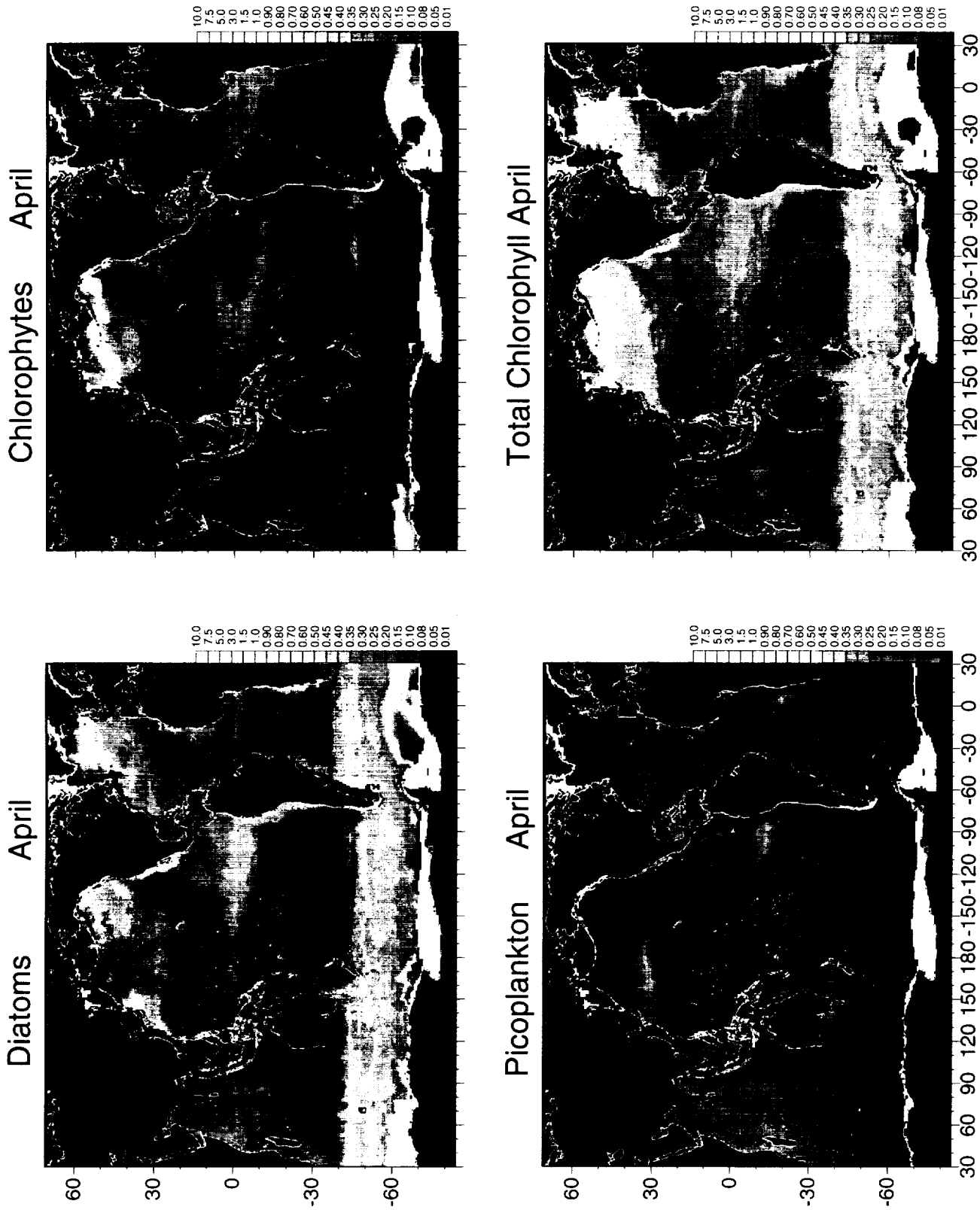

Figure 12. Phytoplankton group distributions and total chlorophyll (sum of the three functional groups) computed for April after 4 years of simulation. These represent values for a single day near the beginning of the month and not monthly means.

Pacific is exceptionally cold, and the success of chlorophytes here is due to their overwintering advantage provided by their lower sinking rates. The cold temperatures suppress maximum growth rates of all groups, but the difference between diatoms and chlorophytes is less in cold water, allowing their lower sinking rates to provide a competitive advantage.

Similar overall distributions of the phytoplankton groups are observed in October as in April, except some facets are reversed in hemisphere (Figure 13). Chlorophytes comprise a larger proportion of the total chlorophyll in the North Pacific and Atlantic. The remnants of the southwest monsoon in the Arabian Sea can be seen and is dominated by diatoms. The southern ocean begins the austral spring bloom and is predominantly diatoms with chlorophytes at the periphery. Picoplankton are again widely distributed and in low abundances, but there are some local blooms such as the edge of the high chlorophyll transition zone in the southern Atlantic.

Diatom dominance of the equatorial Pacific is counter to observations in the region (e.g, Chavez, 1989; Landry et al., 1997; Brown et al., 1999), which indicate a pico-nano-plankton dominated community. The prevalence of nutrients and low chlorophyll, along with associated low biomasses of diatoms in conditions that should support large populations and their associated blooms, is one of the driving influences behind the iron limitation hypothesis. Diatoms appear to be especially subject to iron availability (Miller et al., 1991; Morel et al., 1991a; b; Price et al., 1994). However, diatom abundance has been found to be greater very close to the axis of the Pacific upwelling region (Landry et al., 1997), where iron availability is higher than outside of this band. Since this model does not contain explicit iron regulation, predominance by picoplankton cannot be reproduced. Thus, the model produces phytoplankton group population structure that is reasonable in the absence of iron limitation, and clearly, such effects need to be incorporated in future enhancements.

Seasonal variability of the phytoplankton groups is shown for four regions that are representative of most of the range of the global oceans. The four regions are the North Atlantic (sub-polar region with pronounced spring bloom regions and fall/winter die-off), North Central Pacific (a low chlorophyll biomass central gyre), North Indian Ocean (monsoon-dominated region), and the equatorial Atlantic (representing a tropical upwelling region).

The North Atlantic exhibits a classic pattern of seasonal succession, with diatoms dominating early in the year as the mixed layer begins to shallow and light begins to become available, giving way to dominance by chlorophytes in late summer as the mixed layer stabilizes at shallow depth and nutrients become limiting, and lasting under autumn when fall overturn injects nutrients into the mixed layer and favors diatoms again (Figure 14). Picoplankton provide a low and steady proportion of the total population, but increase slightly in the dead of boreal winter due to reduced losses from sinking and depletion when conditions for growth of diatoms improves.

The North Central Pacific exhibits a similar seasonal succession pattern except that it is between diatoms and picoplankton. The group changeover also occurs earlier in the boreal summer than the North Atlantic. Diatoms are prevalent in winter when mixed layer deepening entrains nutrients, thereby fostering growth. Later in the year, when the mixed layer shallows and nutrients are exhausted, the picoplankton predominate. Chlorophytes in the North Central Pacific maintain low and seasonally invariant populations but are actually changing position latitudinally in response to the enhancement and contraction of the mid-ocean gyre.

The North Indian Ocean is subject to four major seasonal influences: the southwest monsoon peaking in August, the less vigorous northeast monsoon occurring through the boreal winter, and 2 inter-monsoon periods between them (Figure 14). The abundance of diatoms follow the pattern of the monsoons, while picoplankton and chlorophytes respond more favorably to the inter-monsoon seasons. This generally conforms to observations in the region (Brown et al., 1999). In the model, this is due to the presence of nutrients resulting from turbulence and upwelling associated with the monsoon periods and favoring diatom growth. The extent of the diatom dominance is directly related to the strength of the monsoon period: they comprise >80% in the more vigorous southwest monsoon compared to slightly < 50% in the less vigorous northeast monsoon. Losses of diatoms from sinking in the inter-monsoon periods allow chlorophytes and picoplankton to outcompete the diatoms for the low concentrations of nutrients.

The equatorial Atlantic exhibits a very different seasonal pattern than the other regions. In this region, chlorophytes predominate the total chlorophyll throughout the year, yielding to diatoms for only a small period

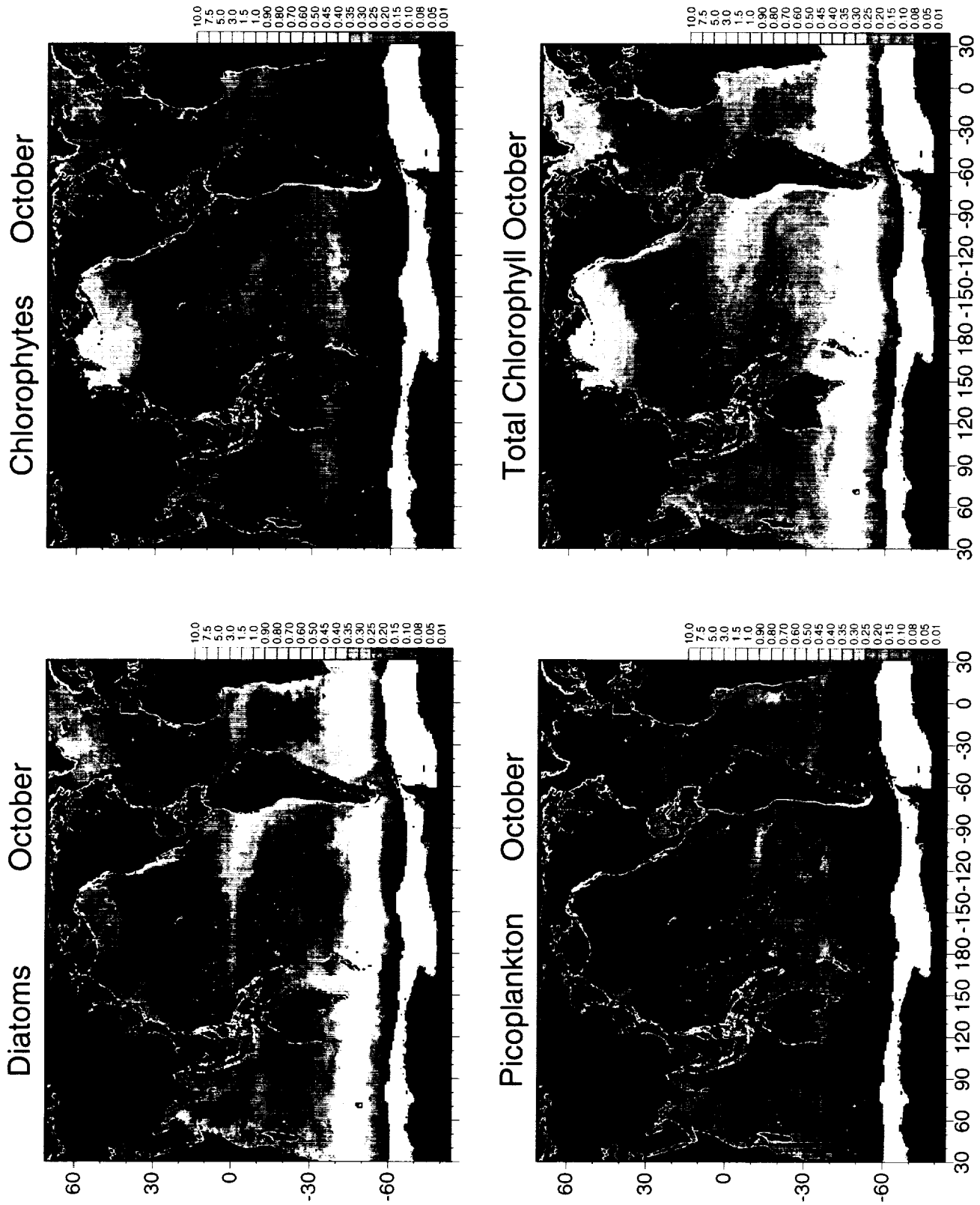

Figure 13. Phytoplankton group distributions and total chlorophyll (sum of the three functional groups) computed for October after 4 years of simulation. These represent values for a single day near the beginning of the month and not monthly means.

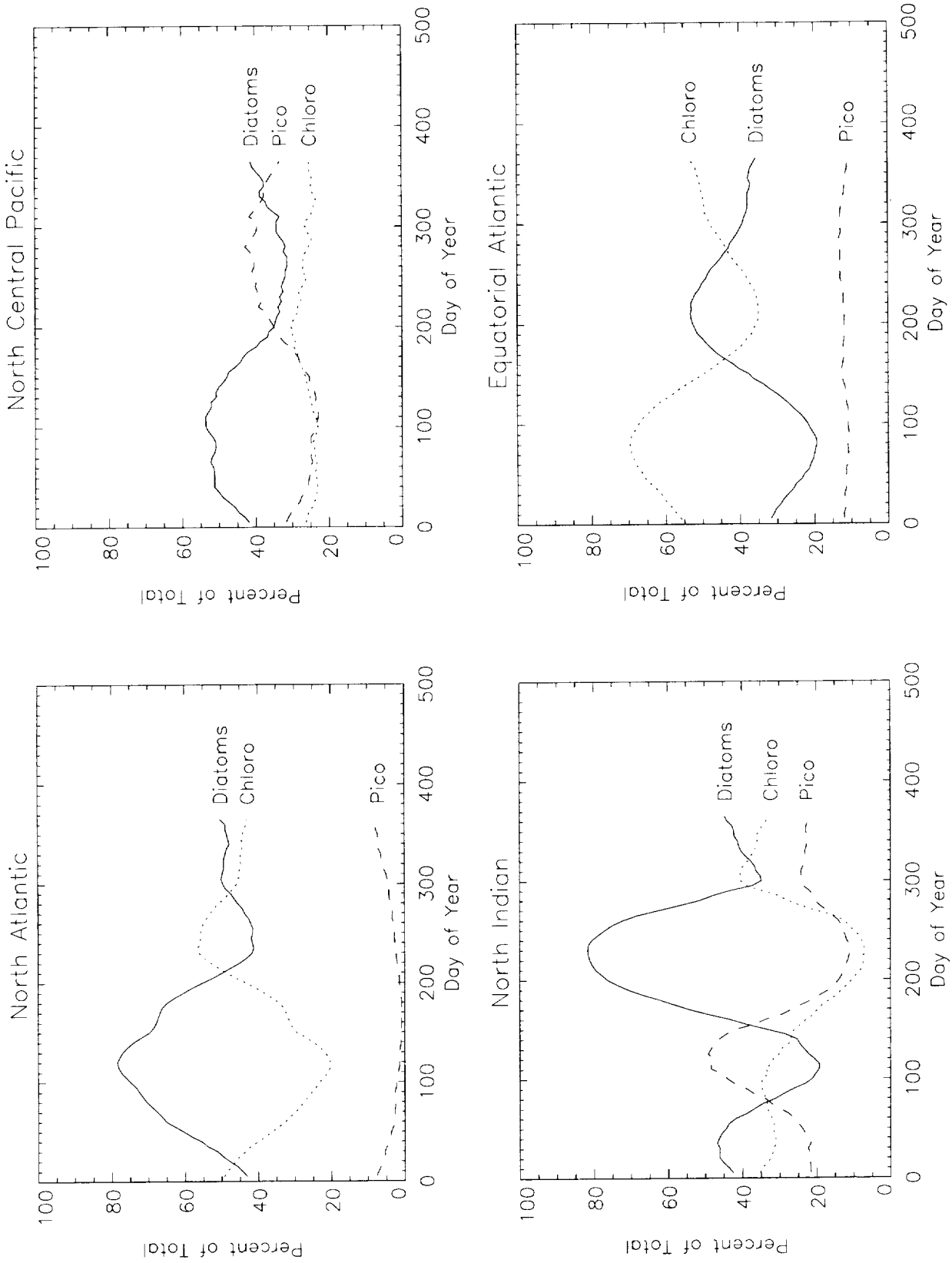

Figure 14. Seasonal variability of phytoplankton groups in 4 regions, chosen to be representative of the range of most conditions in the global oceans. The groups are shown as proportion of the total in percent.

centered about the boreal solstice. These patterns follow the periods of upwelling in the Atlantic (Monger et al., 1997). Overall, picoplankton exhibit very little seasonal variability.

4. SUMMARY AND CONCLUSIONS

Global computed chlorophyll and nitrate distributions from a coupled ocean general circulation, biogeochemical, and radiative model compare with satellite and *in situ* sources. Generally, large-scale chlorophyll features such as the location, size, and shape of mid-ocean gyres, equatorial upwelling regions, high latitudes, and coastal upwelling regions are in agreement with CZCS pigments. Moreover, the seasonal dynamics agree as well. Shifts of high chlorophyll across hemispheres are in correspondence as are timing features of bloom-and-recede. The mid-ocean gyres expand in the local summer and contract in local winter in accordance with mixed layer shallowing and deepening, respectively, and match cycles indicated in the CZCS. Basin scale seasonal trends are in agreement with those determined from the CZCS in every oceanic basin.

Seasonal comparisons with *in situ* nitrate climatologies also exhibit correspondence. The location, seasonal dynamics, and magnitudes are apparent in the model. A notable exception is the equatorial Atlantic upwelling region, which appears prominently in the model but is not indicated in the data.

There are several significant discrepancies between model results and data. For example, the tropical Pacific appears overestimated in the model. Spatial variability in the sub-polar Southern Hemisphere is not represented well by the model. There are processes that may be important such as iron limitation, eddy scale processes, and topographic influences on circulation that are not included in the model. But these discrepancies do not affect the overall agreement of the model with observations at synoptic and basin scales. Considering that the model is initialized with flat fields of chlorophyll, this suggests realism in the physical, biological, and radiative dynamics included in the model, at least at synoptic scales. At times of poor sampling by the CZCS, such as local winter at the high latitudes, the model appears to produce better estimates of chlorophyll concentrations since the CZCS only sampled the portions toward lower latitudes which always had higher estimates. This leads to an overestimate of mean pigment in these seasons, while the model results are unbiased, and incidentally, generally in agreement where small pockets of CZCS sampling occur.

The model contains three phytoplankton groups whose distributions are initialized as equal amounts throughout the model domain. After four years of simulation, they arrive at reasonable distributions throughout the global oceans: diatoms predominate high latitudes, coastal, and equatorial upwelling areas; picoplankton predominate the mid-ocean gyres; and chlorophytes represent a transitional assemblage, occurring predominantly in regions unoccupied by the others. Diatoms are responsible for high chlorophyll regions, while chlorophytes are mostly responsible for seasonal changes in the mid-ocean gyres, i.e., contraction in local winter and expansion in local summer. Seasonal patterns exhibit a range of relative responses: from a classic seasonal succession in the high latitudes with chlorophytes replacing diatoms as the dominant group in mid-summer to successional patterns with picoplankton replacing diatoms in mid-summer in the North Central Pacific. Diatoms are associated with high kinetic energy regions where nutrient availability is high. Picoplankton predominate in quiescent regions with low nutrients. These results are a direct response to differences in phytoplankton group maximum growth and sinking properties. The net effect of the phytoplankton groups is the ability of the model to more accurately represent a wider range of oceanic habitats simultaneously than is possible with a single group. Given that the global ocean is diverse, physically, biologically, and chemically, multiple groups are required to improve simulation accuracy and to represent the major features of seasonal variability.

REFERENCES

Ahn, Y.-H., A. Bricaud, and A. Morel, Light backscattering efficiency and related properties of some phytoplankters, Deep-Sea Res., 39, 1835-1855, 1992.

Arrigo, K.R., D.L. Worthen, M.P. Lizotte, P. Dixon, and G. Dieckmann, Primary production in Antarctic sea ice, Science, 276, 394-397, 1997.

Barlow, R.G. and R.S. Alberte, Photosynthetic characteristics of phycoerythrin-containing marine Synechococcus spp., Mar. Biol., 86, 63-74, 1985.

Bates, S.S. and T. Platt, Fluorescence induction as a measure of photosynthetic capacity in marine phytoplankton: response of *Thalassiosira pseudonana* (Bacillariophyceae) and *Dunaliella tertiolecta* (Chlorophyceae), Mar. Ecol. Prog. Ser., 18, 67-77, 1984.

Ben-Amotz, A. and A. Gilboa, Cryptopreservation of marine unicellular algae. I. A survey of algae with regard to size, culture age, photosynthetic activity and chlorophyll - to - cell ratio. Mar. Ecol. Prog. Ser., 2, 157-161, 1980.

Bissett, W.P., J.J. Walsh, D.A. Dieterle, and K.L. Carder, Carbon cycling in the upper waters of the Sargasso Sea: I. Numerical simulation of differential carbon and nitrogen fluxes, Deep-Sea Res., 46, 205-269, 1999.

Brand, L.E., W.G. Sunda, and R.R.L. Guillard, Reduction of marine phytoplankton reproduction rates by copper and cadmium, J. Exp. Mar. Biol. Ecol., 96, 225-250, 1986.

Brand, L.E., W.G. Sunda, and R.R.L. Guillard, Limitation of marine phytoplankton reproductive rates by zinc, manganese, and iron, Limnol. Oceanogr., 28, 1182-1198, 1983.

Bricaud, A. and A. Morel, Light attenuation and scattering by phytoplanktonic cells: a theoretical modeling, Appl. Opt., 25, 571-580, 1986.

Bricaud, A., A. Morel, and L. Prieur, Optical efficiency factors of some phytoplankters. Limnol. Oceanogr., 28, 816-832, 1983.

Bricaud, A., A.-L. Bedhomme, and A. Morel, Optical properties of diverse phytoplanktonic species: experimental results and theoretical interpretation, J. Plank. Res., 10: 851-873, 1988.

Brown, S.L., M.R. Landry, R.T. Barber, L. Campbell, D.L. Garrison, and M.M. Gowing, Picophytoplankton dynamics and production in the Arabian Sea during the 1995 southwest monsoon, Deep-Sea Res., 46, 1745-1768, 1999.

Carpenter, E.J. and K. Romans, Major role of the cyanobacterium *Trichodesmium* in nutrient cycling in the North Atlantic Ocean, Science , 254, 1356-1358, 1991.

Chai, F., S.T. Lindley, and R.T. Barber, Origin and maintenance of a high nitrate condition in the equatorial Pacific, Deep-Sea Res., 43, 1031-1064, 1996.

Chavez, F.P., Size distribution of phytoplankton in the central and eastern tropical Pacific, Global Biogeochemical Cycles, 3, 27-35, 1989.

Coale, K.H., K.S. Johnson, S.E. Fitzwater, S.O.G. Blain, T.P. Stanton, and T.L. Coley, Iron Ex-I, and *in situ* iron-enrichment experiment: Experimental design, implementation, and results, Deep-Sea Res., 45, 919-945, 1998.

Conkright, M.E., S. Levitus, T.O'Brien, T.P. Boyer, C. Stephens, D. Johnson, L. Stathoplos, O. Baranova, J. Antonov, R. Gelfeld, J. Burney, J. Rochester, and C. Forgy, World Ocean Database 1998 CD-ROM Data Set Documentation, National Oceanographic Data Center, Silver Spring, MD, 1998a.

Conkright, M.E., T.O'Brien, S. Levitus, T.P. Boyer, C. Stephens, J. Antonov, World ocean atlas 1998 Volume 10. Nutrients and chlorophyll of the Atlantic Ocean, NOAA Atlas NESDIS 36, 217pp., 1998b.

Conkright, M.E., T.O'Brien, S. Levitus, T.P. Boyer, C. Stephens, J. Antonov, World ocean atlas 1998 Volume 11. Nutrients and chlorophyll of the Pacific Ocean. NOAA Atlas NESDIS 37, 217pp., 1998c.

Conkright, M.E., T.O'Brien, S. Levitus, T.P. Boyer, C. Stephens, J. Antonov, World ocean atlas 1998 Volume 12. Nutrients and chlorophyll of the Indian Ocean. NOAA Atlas NESDIS 38, 217pp., 1998d.

Conkright, M.E., S. Levitus and T.P. Boyer, World Ocean Atlas, Volume 1: Nutrients, NOAA Atlas NESDIS 1, 150 pp., 1994a.

Conkright, M.E., S. Levitus and T.P. Boyer, Quality Control of Historical Nutrient Data., NOAA Technical Memorandum 79, 75 pp., 1994b.

Csanady, G.T., Mass transfer to and from small particles in the sea, Limnol. Oceangr., 31,237-248,1986.

Da Silva, A.M., C.C. Young, and S. Levitus, Atlas of surface marine data 1994 Volume 1: Algorithms and procedures, NOAA Atlas NESDIS 6, 83 pp., 1994.

Dubinsky, Z. and T. Berman, Light utilization efficiencies of phytoplankton in Lake Kinneret (Sea of Galilee), Limnol. Oceanogr., 21, 226-230, 1986.

Dugdale, R.C. and J.J. Goering, Uptake of new and regenerated forms of nitrogen in primary productivity, Limnol. Oceanogr., 12, 196-206, 1967.

Dutkiewicz, S., M. Follows, J. Marshall, and W.W. Gregg, Interannual variability of phytoplankton abundances in the North Atlantic. Deep-Sea Research, in press, 2000.

Eppley, R.W., Temperature and phytoplankton growth in the sea, Fish. Bull., 70, 1063-1085, 1972.

Eppley, R.W., J.N. Rogers, and J.J. McCarthy, Half-saturation constants for uptake of nitrate and ammonium by marine phytoplankton, Limnol. Oceanogr., 14, 912-920, 1969

Eppley, R.W. and B.J. Peterson, Particulate organic matter flux and planktonic new production in the deep ocean, Nature, 282, 677-680, 1979.

Eynaud, F., J. Girardeau, J.-J. Pichon, and C.J. Pudsey, Sea-surface distribution of coccolithophores, diatoms, silicoflagellates, and dinoflagellates in the South Atlantic Ocean during the late austral summer 1995, Deep-Sea Res., 46, 451-482, 1999.

Fasham, M.J.R., J.L. Sarmiento, R.D. Slater, H.W. Ducklow, and R. Williams, A seasonal three-dimensional ecosystem model of nitrogen cycling in the North Atlantic euphotic zone: A comparison of the model results with observations from Bermuda Station "S" and OWS "India", Global Biogeochem. Cycles, 7, 379-415, 1993.

Furnas, M.J., Net *in situ* growth rates of phytoplankton in an oligotrophic, tropical shelf ecosystem, Limnol. Oceanogr., 36, 13-29, 1991.

Gardner, W.D., J.S. Gundersen, M.J. Richardson, and I.D. Walsh. The role of seasonal and diel changes in mixed-layer depth on carbon and chlorophyll distributions in the Arabian Sea. Deep-Sea Res. 46: 1833-1858, 1999.

Gavis, J., R.R.L. Guillard, and B.L. Woodward, Cupric ion activity and the growth of phytoplankton clones isolated from different marine environments, J. Mar. Res., 39, 315-333, 1981.

Glover, H.E., The physiology and ecology of the marine cyanobacterial genus *Synechococcus*, Adv. Microbiol., 3, 49-107, 1985.

Goldman, J.C. and P.M. Glibert, Comparative rapid ammonium uptake by four species of marine phytoplankton, Limnol. Oceanogr., 27, 814-827, 1982.

Gregg, W.W. and K.L. Carder, A simple spectral solar irradiance model for cloudless maritime atmospheres, Limnol. Oceanogr., 35, 1657-1675, 1990.

Gregg, W.W. and J.J. Walsh, Simulation of the 1979 spring bloom in the Mid-Atlantic Bight: A coupled physical/ biological/optical model, J. Geophys. Res., 97, 5723-5743, 1992.

Gregg, W.W., Radiative impacts of clouds on phytoplankton growth, Global Change Biol., submitted, 2000.

Humphrey, G.F., Photosynthetic characteristics of algae grown under constant illumination and light-dark regimes, J. Exp. Mar. Biol. Ecol., 40, 63-70, 1979.

Itturiaga, R. and B.G. Mitchell, Chrococcoid cyanobacteria: a significant component in the food web dynamics of the open ocean, Mar. Ecol. Prog. Ser., 28, 291-297, 1986.

Itturiaga, R. and J. Marra, Temporal and spatial variability of chroccoid cyanobacteria *Synechococcus* spp. specific growth rates and their contribution to primary productivity in the Sargasso Sea, Mar. Ecol. Prog. Ser., 44, 175-181, 1988.

Kiefer, D.A. and B.G. Mitchell, A simple, steady state description of phytoplankton growth based on absorption cross section and quantum efficiency, Limnol. Oceanogr., 28, 770-775, 1983.

Kirk, J.T.O., Spectral properties of natural waters: Contribution of the soluble and particulate fractions to light absorption in some inland waters of southeastern Australia, Australian Journal of Marine and Freshwater Research, 31, 287-296, 1980.

Kolber, Z.S., R.T. Barber, K.H. Coale, S.E. Fitzwater, R.M. Greene, K.S. Johnson, S. Lindley, and P.G. Falkowski, Iron limitation of phytoplankton photosynthesis in the equatorial Pacific Ocean, Nature, 371, 145-148, 1994.

Landry, M.R., R.T. Barber, R.R. Bidigare, F. Cahi, K.H. Coale, H.G. Dam, M.R. Lewis, S.T. Lindley, J.J. McCarthy, M.R. Roman, D.K. Stoecker, P.G. Verity, and J.R. White, Iron and grazing constraints on primary production in the central equatorial Pacific: An EqPac synthesis. Limnol. Oceanogr., 42, 405-418, 1997.

Langdon, C., On the causes of interspecific differences in the growth-irradiance relationship for phytoplankton. Part I. A comparative study of the growth-irradiance relationship of three marine phytoplankton species: *Skeletonema costatum, Olisthodiscus luteus, and Gonyaulax tamarensis*, J. Plank. Res., 9, 459-482, 1987.

Levitus, S. and T.P. Boyer, World ocean atlas 1994, Volume 4: temperature. NOAA Atlas NESDIS 4, US Dept. of Commerce, Washington, DC, 117 pp., 1994.

Levitus, S., R. Burgett, and T.P. Boyer, World ocean atlas 1994, Volume 3: salinity. NOAA Atlas NESDIS 3, US Dept. of Commerce, Washington, DC, 93 pp., 1994.

Longhurst, A., Seasonal cycles of pelagic production and consumption, Prog. Oceangr., 35, 77-167, 1995.

Martin, J.H. and S.E. Fitzwater, Iron deficiency limits phytoplankton growth in the north-east Pacific subarctic, Nature, 331, 341-343, 1988.

Martin, J.H., R.M. Gordon, and S.E. Fitzwater, Iron in Antarctic waters, Nature, 345, 156-158, 1990.

McGillicuddy, D.J., J.J. McCarthy, and A.R. Robinson, Coupled physical and biological modeling of the spring bloom in the North Atlantic (I): Model formulation and one dimensional bloom processes, Deep-Sea Res., 42, 1313-1357, 1995b.

McGillicuddy, D.J., A.R. Robinson, and J.J.McCarthy, Coupled physical and biological modelling of the spring bloom in the North Atlantic (II): three dimensional bloom and post-bloom processes. Deep-Sea Research, 8, 1359-1398, 1995a.,

McNeil, A.F. Michaels, and A.H. Knap, Influence of mesoscale eddies on new production in the Sargasso Sea, Nature, 394, 263-266, 1998.

Miller, C.B. and others, Ecological dynamics in the subarctic Pacific, a possibly iron-limited system, Limnol. Oceanogr., 36, 1600-1615, 1991.

Mitchell, B.G. and D.A. Kiefer, Chlorophyll a specific absorption and fluorescence excitation spectra for light-limited phytoplankton, Deep-Sea Res., 35, 639-663, 1988.

Monger, B., C. McClain, and R. Murtugudde, Seasonal phytoplankton dynamics in the eastern tropical Atlantic, J. Geophys. Res., 102, 12389-12411, 1997.

Morel, A., Chlorophyll-specific scattering coefficient of phytoplankton. A simplified theoretical approach, Deep-Sea Res., 34, 1093-1105, 1987.

Morel, A. and A. Bricaud, Theoretical results concerning light absorption in a discrete medium, and application to specific absorption of phytoplankton, Deep-Sea Res., 28, 1375-1393, 1981.

Morel, F.M.M., R.J.M. Hudson, and N.M. Price, Limitation of productivity by trace metals in the sea, Limnol. Oceanogr., 36, 1742-1755, 1991a.

Morel, F.M.M., J.G. Rueter, and N.M. Price, Iron nutrition of phytoplankton and its possible importance in the ecology of open ocean regions with high nutrient and low biomass, Oceanography, 4, 56-61, 1991b.

O'Reilly, J.E., S. Maritorena, B.G. Mitchell, D.A. Siegel, K.L. Carder, S.A. Garver, M. Kahru, and C. McClain, Ocean color chlorophyll algorithms for SeaWiFS. J. Geophys. Res., 103, 24937-24953, 1998.

Oschlies, A. and V. Garcon, Eddy-induced enhancement of primary production in a model of the North Atlantic Ocean, Nature, 394, 266-269, 1998.

Pacanowski, R.C. and G. Philander, Parameterization of vertical mixing in numerical models of the tropical ocean, J. Phys. Oceanogr., 11, 1442-1451, 1981.

Perry, M.J., M.C. Talbot, and R.S. Alberte, Photoadaptation in marine phytoplankton: response of the photosynthetic unit, Mar. Biol., 62, 91-101, 1981.

Platt, T., C. Caverhill, and S. Sathyendranath, Basin-scale estimates of oceanic primary production by remote sensing: The North Atlantic, J. Geophys. Res., 96, 15147-15159, 1991.

Pribble, J.R., J.J. Walsh, D.A. Dieterle, and F.E. Muller-Karger, Numerical analysis of shipboard and coastal zone color scanner time series of new production within Gulf Stream cyclonic eddies in the South Atlantic Bight, J. Geophys. Res., 99, 7513-7538, 1994.

Price, N.M., B.A. Ahner, and F.M.M. Morel, The equatorial Pacific Ocean: Grazer-controlled phytoplankton populations in an iron-limited ecosystem, Limnol. Oceanogr., 39, 520-534, 1994.

Roache, P.J., Computational Fluid Dynamics, Hermosa Publ., Albuquerque, NM., 446 pp., 1982.

Sakshaug, E. and K. Andresen, Effect of light regime upon growth rate and chemical composition of a clone of Skeletonema costatum from the Trondheimsfjord, Norway, J. Plank. Res., 8, 619-637, 1986.

Sarmiento, J.L., R.D. Slater, M.J.R. Fasham, H.W. Ducklow, J.R. Toggweiler, and G.T. Evans, A seasonal three-dimensional ecosystem model of nitrogen cycling in the North Atlantic euphotic zone. Glob. Biogeochem. Cycles, 7, 417-450, 1993

Sathyendranath, S., L. Lazzara, and L. Prieur, Variations in the spectral values of specific absorption of phytoplankton. Limnol. Oceanogr., 32, 403-415, 1987.

Sathyendranath, S., A. Longhurst, C.M. Caverhill, and T. Platt, Regionally and seasonally differentiated primary production in the North Atlantic, Deep-Sea Res., 42, 1773-1802, 1995.

Schopf, P.S. and A. Loughe, A reduced gravity isopycnal ocean model: Hindcasts of El Nino, Mon. Wea. Rev., 123, 2839-2863, 1995.

Slingo, A., A GCM parameterization for the shortwave radiative properties of water clouds, J. Atmos. Sci., 46, 1419-1427, 1989.

Subba Rao, D.V., Growth response of marine phytoplankton to selected concentrations of trace metals, Botanica marina, 24, 369-379, 1981.

Toggweiler, J.R. and S. Carson, What are upwelling systems contributing to the ocean's carbon and nutrient budgets?, pp. 3137-369 In: Upwelling in the ocean: modern processes and ancient record, C.P. Summerhayes, M.V. Angel, R.L. Smith, and B. Zeitzschel, eds. J. Wiley and Sons, New York.

Walsh, J.J., D.A. Dieterle, F.E. Muller-Karger, R. Bohrer, W.P. Bissett, R.J. Varela, R. Aparicio, R. Diaz, R. Thunell, G.T. Taylor, M.I. Scranton, K.A. Fanning, and E.T. Peltzer, Simulation of carbon-nitrogen cycling during spring upwelling in the Cariaco Basin, J. Geophys. Res., 104, 7807-7825, 1999.

Wyman, M. and P. Fay, Underwater light climate and the growth and pigmentation of planktonic blue-green algae (Cyanobacteria) I. The influence of light quantity, Proc. R. Soc. Lond. 227, 367-380, 1986.

Yoder, J.A., C.R. McClain, G.C. Feldman, and W.E. Esaias, Annual cycles of phytoplankton chlorophyll concentrations in the global ocean: a satellite view. Global Biogeochem. Cycles, 7, 181-193, 1993.

REPORT DOCUMENTATION PAGE

Form Approved
OMB No. 0704-0188

1. AGENCY USE ONLY *(Leave blank)*	2. REPORT DATE	3. REPORT TYPE AND DATES COVERED
	September 2000	Technical Memorandum

4. TITLE AND SUBTITLE
A Coupled Ocean General Circulation, Biogeochemical, and Radiative Model of the Global Oceans: Seasonal Distributions of Ocean Chlorophyll and Nutrients

5. FUNDING NUMBERS
Code 971

6. AUTHOR(S)
Watson W. Gregg

7. PERFORMING ORGANIZATION NAME(S) AND ADDRESS (ES)
Laboratory for Hydrospheric Processes
Goddard Space Flight Center
Greenbelt, Maryland 20771

8. PEFORMING ORGANIZATION REPORT NUMBER
2000-03905-0

9. SPONSORING / MONITORING AGENCY NAME(S) AND ADDRESS (ES)
National Aeronautics and Space Administration
Washington, DC 20546-0001

10. SPONSORING / MONITORING AGENCY REPORT NUMBER
TM-2000-209965

11. SUPPLEMENTARY NOTES

12a. DISTRIBUTION / AVAILABILITY STATEMENT
Unclassified–Unlimited
Subject Category: 48
Report available from the NASA Center for AeroSpace Information,
7121 Standard Drive, Hanover, MD 21076-1320. (301) 621-0390.

12b. DISTRIBUTION CODE

13. ABSTRACT *(Maximum 200 words)*

A coupled ocean general circulation, biogeochemical, and radiative model was constructed to evaluate and understand the nature of seasonal variability of chlorophyll and nutrients in the global oceans. Biogeochemical processes in the model are determined from the influences of circulation and turbulence dynamics, irradiance availability, and the interactions among three functional phytoplankton groups (diatoms, chlorophytes, and picoplankton) and three nutrients (nitrate, ammonium, and silicate).

Basin scale (>1000 km) model chlorophyll results are in overall agreement with CZCS pigments in many global regions. Seasonal variability observed in the CZCS is also represented in the model. Synoptic scale (100-1000 km) comparisons of imagery are generally in conformance although occasional departures are apparent. Model nitrate distributions agree with *in situ* data, including seasonal dynamics, except for the equatorial Atlantic. The overall agreement of the model with satellite and *in situ* data sources indicates that the model dynamics offer a reasonably realistic simulation of phytoplankton and nutrient dynamics on synoptic scales. This is especially true given that initial conditions are homogenous chlorophyll fields.

The success of the model in producing a reasonable representation of chlorophyll and nutrient distributions and seasonal variability in the global oceans is attributed to the application of a generalized, processes-driven approach as opposed to regional parameterization and the existence of multiple phytoplankton groups with different physiological and physical properties. These factors enable the model to simultaneously represent many aspects of the great diversity of physical, biological, chemical, and radiative environments encountered in the global oceans.

14. SUBJECT TERMS
ocean modeling, biochemical processes, ocean chlorophyll, nutrients

15. NUMBER OF PAGES
33

16. PRICE CODE

17. SECURITY CLASSIFICATION OF REPORT	18. SECURITY CLASSIFICATION OF THIS PAGE	19. SECURITY CLASSIFICATION OF ABSTRACT	20. LIMITATION OF ABSTRACT
Unclassified	Unclassified	Unclassified	UL